Inorganic Chemistry

pubs.acs.org/IC Article

Chelation in One Fell Swoop: Optimizing Ligands for Smaller Radiometal Ions

Neha Choudhary, María de Guadalupe Jaraquemada-Peláez, Kristof Zarschler, Xiaozhu Wang, Valery Radchenko, Manja Kubeil, Holger Stephan, and Chris Orvig*

Cite This: https://dx.doi.org/10.1021/acs.inorgchem.0c00509 Read Online

ACCESS | Metrics & More | Article Recommendations | Supporting Information

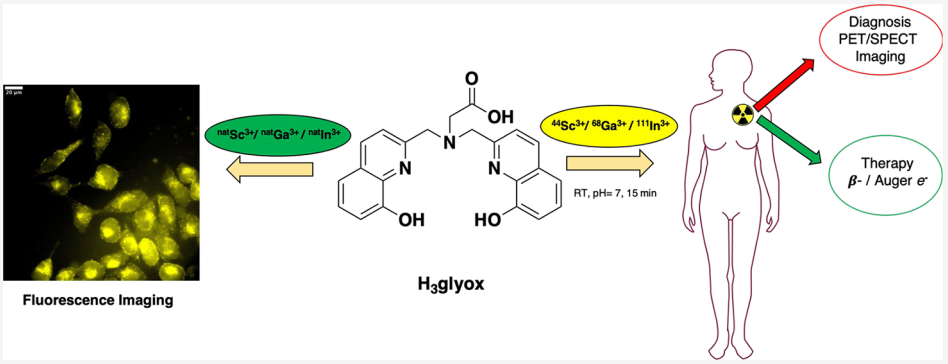

ABSTRACT: [$^{44/47}$Sc]Sc^{3+}, [^{68}Ga]Ga^{3+}, and [^{111}In]In^{3+} are the three most attractive trivalent smaller radiometalnuclides, offering a wide range of distinct properties (emission energies and types) in the toolbox of nuclear medicine. In this study, all three of the metal ions are successfully chelated using a new oxine-based hexadentate ligand, H_3glyox, which forms thermodynamically stable neutral complexes with exceptionally high pM values [pIn (34) > pSc (26) > pGa (24.9)]. X-ray diffraction single crystal structures with stable isotopes revealed that the ligand is highly preorganized and has a perfect fit to size cavity to form [Sc(glyox)(H_2O)] and [In(glyox)(H_2O)] complexes. Quantitative radiolabeling with gallium-68 (RCY > 95%, [L] = 10^{-5} M) and indium-111 (RCY > 99%, [L] = 10^{-8} M) was achieved under ambient conditions (RT, pH 7, and 15 min) with very high apparent molar activities of 750 MBq/μmol and 650 MBq/nmol, respectively. Preliminary quantitative radiolabeling of [^{44}Sc]$ScCl_3$ (RCY > 99%, [L] = 10^{-6} M) was fast at room temperature (pH 7 and 10 min). *In vitro* experiments revealed exceptional stability of both [^{68}Ga]Ga(glyox) and [^{111}In]In(glyox) complexes against human serum (transchelation <2%) and its suitability for biological applications. Additionally, on chelation with metal ions, H_3glyox exhibits enhanced fluorescence, which was employed to determine the stability constants for Sc(glyox) in addition to the in-batch UV−vis spectrophotometric titrations; as a proof-of-concept these complexes were used to obtain fluorescence images of live HeLa cells using Sc(glyox) and Ga(glyox), confirming the viability of the cells. These initial investigations suggest H_3glyox to be a valuable chelator for radiometal-based diagnosis (nuclear and optical imaging) and therapy.

INTRODUCTION

Since Alexander Graham Bell suggested placing a radium source in or near tumors to treat them in 1903, radioisotopes have been widely used for many applications in physiology and biochemistry, including treatment of benign and malignant tumors.[1] The development of [^{18}F]FDG and many ^{99m}Tc complexes for positron emission tomography (PET) and single photon emission computed tomography (SPECT), respectively, revolutionized the practice of nuclear medicine, and these two types of drugs are routinely used diagnostically in the clinic.[2,3]

The rapid and successful growth of nuclear medicine is also owed to advances in detector technologies and isotope production methods using biomedical generators and cyclotrons; this has led to the availability of diverse medicinally useful radiometals with varying physical (half-life, specific activity, emission type) and chemical (hardness, oxidation state, acidity) properties and has stimulated research interest in harnessing the potential of radiometals for diagnostic imaging as well as use of the emitted particles "millions of tiny bullets of energy" (α-particles, β^- particles, and Auger electrons) for therapy to kill well-targeted cancerous cells.[4−11] Scandium-44 and gallium-68 are two significant PET radionuclides (^{44}Sc, $E\beta_{avg}^+$ = 632 keV, 94%; ^{68}Ga, $E\beta_{avg}^+$ = 830 keV, 89%)

Received: February 17, 2020

Chart 1. Structures of Ligands Discussed

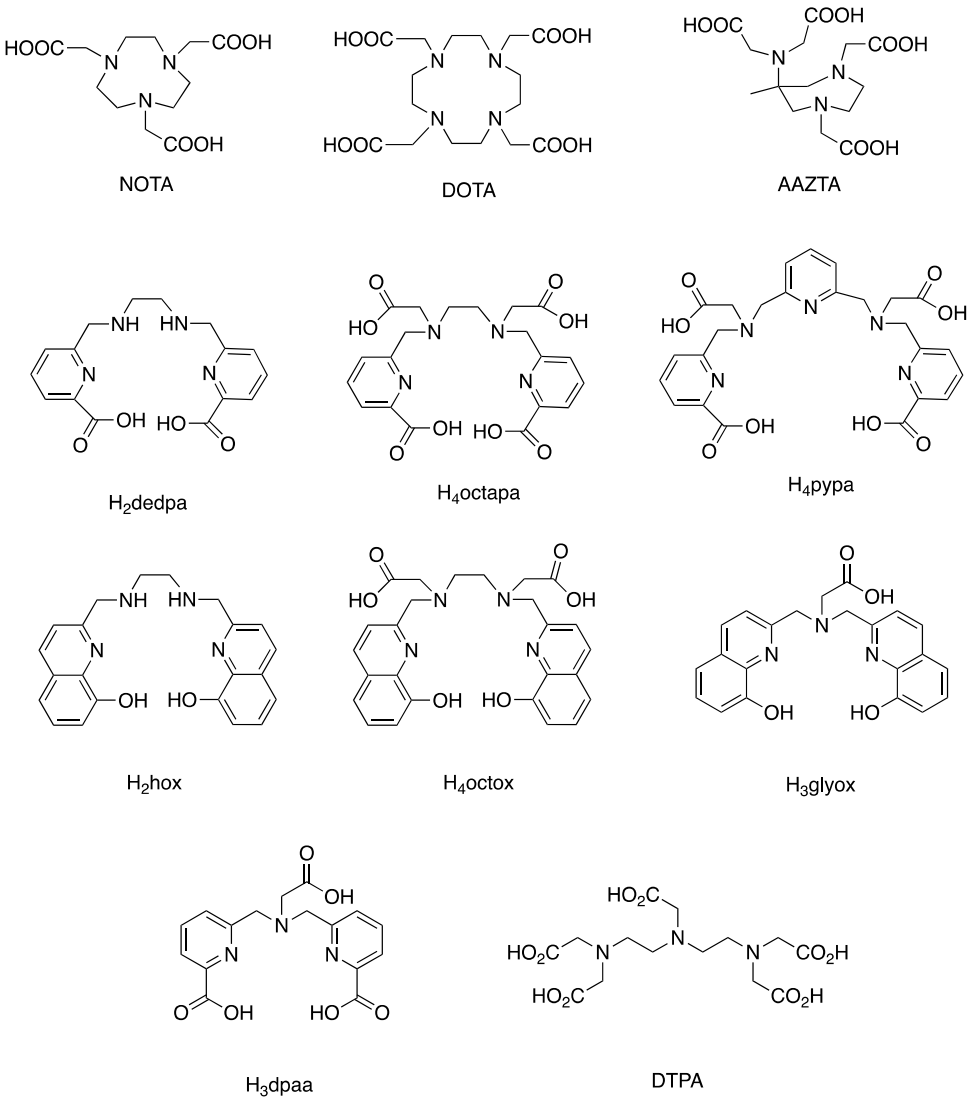

attracting attention because of the convenience of their availability using ^{44}Ti/^{44}Sc and ^{68}Ge/^{68}Ga generator systems, respectively.[12−15] Scandium-44 has a longer physical half-life ($t_{1/2}$ = 4.04 h) as compared to that of gallium-68 ($t_{1/2}$ = 68 min), advantageous for acquisition of images at later time points.[16−18] Substantial advantages of the scandium-44/47 pair as a theranostic combination are the identical chemistries but different emission types and energies of the two radioisotopes. Scandium-47 is a β^- emitter ($E\beta^-_{avg}$= 162 keV, 100%; $t_{1/2}$ = 80.4 h) suitable for the treatment of localized cancerous cells.[19] Eppard et al. recently confirmed the suitability of [^{44}Sc]Sc-PSMA-617 for PET imaging and the pretherapeutic dosimetry of prostate cancer in human patients.[20] Indium-111 ($E\gamma$ = 171 and 245 keV, $t_{1/2}$= 67.2 h) is a radionuclide of long-standing in SPECT imaging agents; it has found its firm place in clinical use. ^{111}In-labeled oxyquinoline, Octreoscan, Prostascint, and MPI indium DTPA (diethylenetriamine pentaacetic acid) In111 (Pentetate Indium Disodium In111) are examples of FDA-approved ^{111}In-based radiopharmaceuticals.[21] Indium-110m is another relevant radioisotope for PET imaging;[22] researchers also have a keen interest in using Auger electrons emitted by indium-111 for therapy.[23,24]

The development of radiometal-based imaging and therapy heavily relies on the use of bifunctional chelators (BFCs) that sequester the radiometal ion from aqueous solution and transport, via conjugation to targeting vectors (antibodies, peptides etc.),[25] to the desired site *in vivo*. Therefore, an in-depth study of the chelator and its metal complex is required to determine the thermodynamic stability and kinetic inertness and avoid any transchelation with the endogenous ligands present in the body; radiolabeling must preferably be fast under ambient conditions. It is an added advantage if one single ligand can be used as a probe for chelating different radiometals as per the need. Therefore, it is of the utmost importance to explore the chemistry of the ligand and the metal complex, remembering Pearson's HSAB principle.[26]

Ga^{3+} is a hard acid (I_A = 7.07) with ionic radius 47−62 pm and a preference for coordination number 4−6.[27] Many macrocyclic and nonmacrocyclic ligands (examples appear in Chart 1) have been reported for their applications in $^{67/68}$Ga based radiopharmaceuticals.[28−34] DOTA (1,4,7,10-tetraazacyclododecane-1,4,7,10-tetraacetic acid) still remains the chelator most widely used by clinicians to radiolabel $^{68}Ga^{3+}$, but at elevated temperatures—conditions antithetical to using antibodies as a delivery vehicle—because of the significant

https://dx.doi.org/10.1021/acs.inorgchem.0c00509
Inorg. Chem. XXXX, XXX, XXX−XXX

Scheme 1. Synthesis of H_3glyox, 3

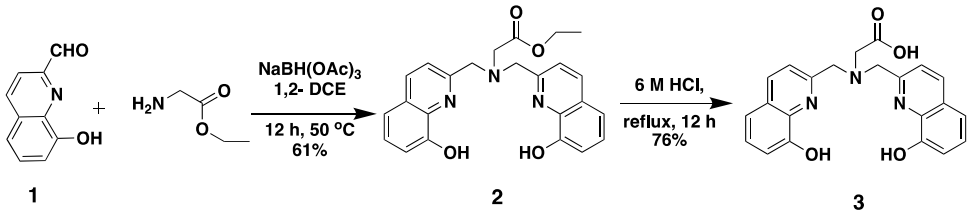

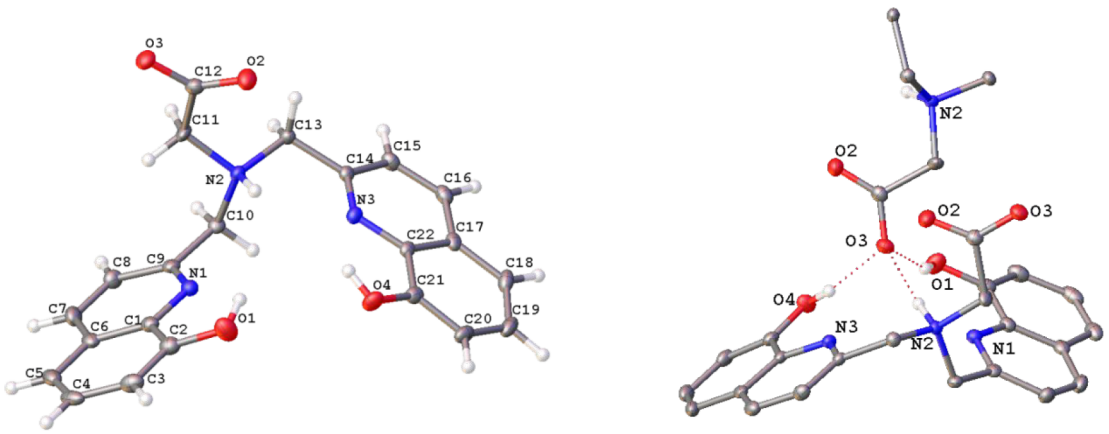

Figure 1. ORTEP diagram of H_3glyox (left) and intermolecular (two ligand molecules) hydrogen bonding in H_3glyox (right). Ellipsoids are shown at the 50% probability level. The following color code was used: C, gray; H, white; N, blue; O, red.

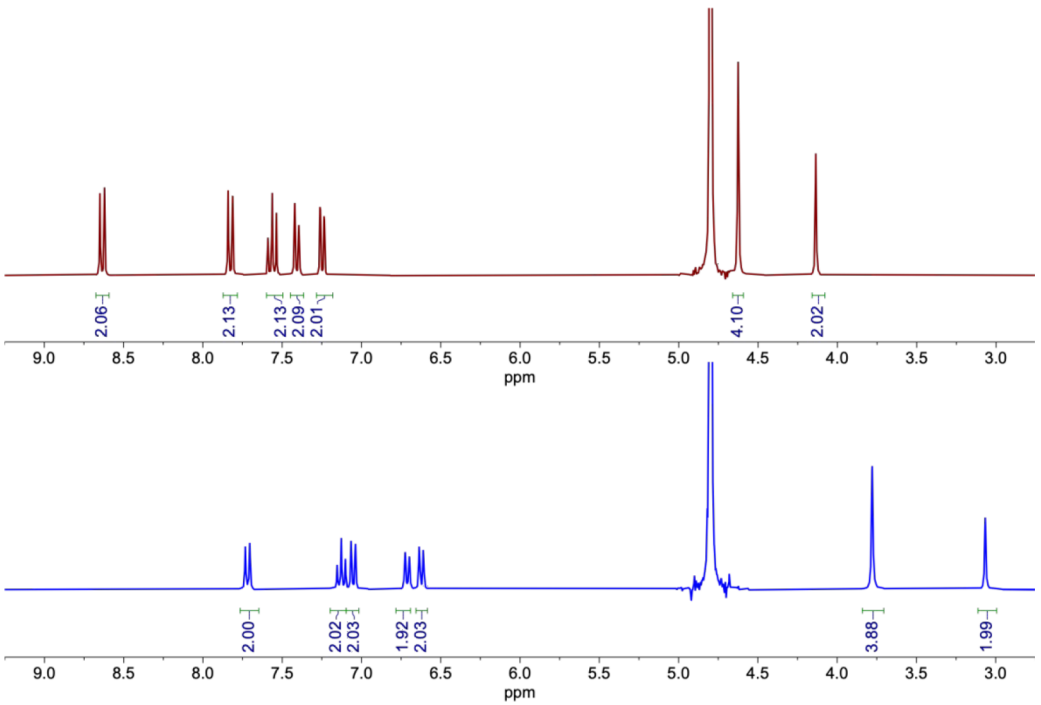

Figure 2. ^{1}H NMR (300 MHz, room temperature, D_2O, pD = 7) spectra of the ligand, H_3glyox (top in red), and Ga(glyox) (bottom in blue).

thermodynamic stability and kinetic inertness of the $[Ga(DOTA)]^-$ complex.

The chemistry of Sc^{3+} has resemblance to both the first-row transition and lanthanide metal ions. Sc^{3+} is the smallest rare-earth metal acid, with an ionic radius of 75−87 pm[27] but is a slightly larger metal ion than is Ga^{3+} and has a very strong preference for hard ligating atoms. Ga^{3+} and In^{3+} belong to group 13 in the periodic table, but In^{3+} is considered a softer acidic metal ion (I_A = 6.3) when compared with Ga^{3+} (I_A = 7.07) and Sc^{3+} (I_A = 10.49), with a larger ionic radius 62−92 pm and preferred coordination number 6−8.[27]

Herein, we discuss our efforts to develop a universal chelator for smaller to medium size trivalent ions, one which forms thermodynamically stable and kinetically inert complexes with all three of our selected trivalent (radio)metal ions (Sc^{3+}, Ga^{3+} and In^{3+}), to offer distinctive decay properties and share

https://dx.doi.org/10.1021/acs.inorgchem.0c00509
Inorg. Chem. XXXX, XXX, XXX−XXX

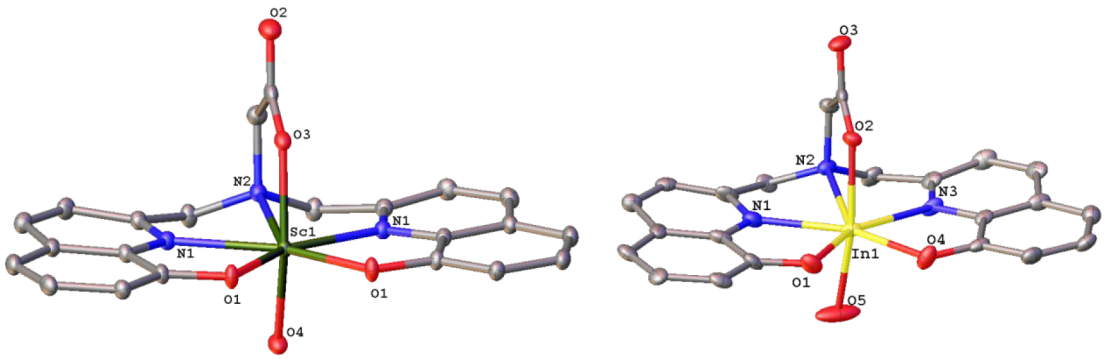

Figure 3. ORTEP diagrams of [Sc(glyox)(H_2O)] (left) and [In(glyox)(H_2O)] (right). Ellipsoids are shown at the 50% probability level; cocrystallized solvent molecules and hydrogen atoms are omitted for clarity. The following color code was used: C, gray; N, blue; O, red; Sc, green; In, yellow.

coordination preferences. These metal complexes can be potentially used for PET and SPECT imaging for diagnosis, and for therapy, with the additional property of metal chelation enhanced fluorescence—a potential imaging modality for molecular and cellular targets. Using the single amino acid approach,[35] the hexadentate chelator H_3glyox was synthesized inspired by the H_3dpaa ligand and the "ox" family ligands, H_2hox and H_4octox.[32,36−38] The ligand scaffold consists of two rigid 8-hydroxyquinoline (ox-arm) binding motifs connected via methylene bridges at the 2 position of each oxine motif to a central nitrogen atom from the glycine amino acid, resulting in an open chain hexadentate chelating system. Furthermore, the glycine backbone provides a convenient site for the functionalization using different amino acids which can be conjugated to targeting vectors.[36,39] Another major aim of this research work is to evaluate the effect of the overall charge of the metal complex on the behavior of the radiotracer in terms of lipophilicity and thermodynamic stability constants as the ligand forms charge-neutral metal complexes with the trivalent metal ions (Sc^{3+}, Ga^{3+}, and In^{3+}).

RESULTS AND DISCUSSION

Synthesis and Characterization. The highly preorganized hexadentate ligand, H_3glyox, was synthesized in two steps using the double reductive amination reaction of 8-hydroxyquinoline-2-aldehyde with glycine ethyl ester hydrochloride using $NaBH(OAc)_3$ as the mild reducing agent, followed by deprotection of the carboxylic group under acidic conditions (Scheme 1). The product ligand was characterized by ^{1}H and ^{13}C NMR spectroscopy and HR-MS, with the purity confirmed by elemental analysis. Needle-like crystals of H_3glyox were obtained from its solution in water and acetonitrile. The preorganization of the ligand can be seen from the crystal structure (Figure 1) in its zwitterionic form. The X-ray diffraction analysis showed that there is an intensive intermolecular H-bonding between the O3 atom from the carboxylic group (another molecule of the ligand, see Figure 1) and the H atom bonded to the N2 atom of the backbone and the H atoms attached to phenolic−OH (O1 and O4) of the oxine arms. These strong hydrogen bonding interactions preorganize the ligand for chelation as compared to an open chain structure such as the H_2hox ligand; preorganization eventually leads to faster complexation rates.[32]

Metal Complexation. The metal complexes were prepared by directly mixing aqueous solutions of H_3glyox and the corresponding metal salts ($ScCl_3$, $Ga(ClO_4)_3$, and $In(ClO_4)_3$); the pH was adjusted to 7 using 0.1 M NaOH. Metal complexation was confirmed by HR-MS as well as ^{1}H NMR spectroscopy. It can be seen in Figure 2 that on complexation with Ga^{3+} there is an upfield chemical shift for all the protons of the ligand due to shielding provided by the electrons of the Ga^{3+} ion. In contrast to the $[Ga(hox)]^+$ and Ga(dpaa) complexes, there is no diastereotopic splitting observed for the methylene protons, which indicates the low energy barriers for the metal-chelate ring inversion—their behavior can be considered fluxional and symmetrical in solution.[32,37] The ^{1}H NMR spectrum along with no change in the number of peaks in the ^{13}C NMR spectrum of the ligand H_3glyox observed upon Ga^{3+} coordination together suggest that no chemically distinct isomers (possibly of differing coordination numbers) were formed at room temperature (Figure S26). Due to the poor solubility of the analogous Sc(glyox) and In(glyox) complexes, the ^{1}H NMR peak signals are not that strong, but change in chemical shifts can be seen in the aromatic region (Figure S11).

X-ray Crystal Structures of Metal Complexes. Structure visualization is a key step in understanding the physiological and pharmacokinetic behavior of the metal complexes. Seven-coordinate metal complexes are far fewer in the literature than 4−6 coordinate analogues. In particular for In^{3+} only a handful of structures have been reported, and this work makes a significant addition.[40−44] Owing to their relatively similar size and preference for coordination numbers 6−8, both Sc^{3+} (0.74 Å, CN-6) and In^{3+} (0.80 Å, CN-6) metal ions form very similar hepta-coordinated complexes with hexadentate $glyox^{3-}$ plus a water molecule.[27]

The geometry around the metal ion can be described as slightly distorted pentagonal bipyramidal in which the ligand adopts a pincer-like arrangement around the metal center with the two 8-hydroxyquinoline arms coplanar, the N2 atom of the backbone slightly pushed out of the plane, and the axial sites occupied by a water molecule and oxygen atom from the carboxylic group. The structures shown in Figure 3 depict a perfect fit of the metal ions into the pocket of the preorganized ligand. It can be noted that the Sc−O_{oxine} bond distances (2.123 Å, see Table 1) are shorter than the Sc−N_{oxine} analogs (2.285 Å, see Table 1), which can be explained by the higher ionic binding affinity of Sc^{3+}, it being the smallest rare earth metal and consistent with the bond distances previously reported in the eight coordinated structures of $[Sc(DOTA)]^-$, $[Sc(DTPA)]^{2-}$, $[Sc_2(oxalate)_7]^{8-}$, and $[Sc(AAZTA)(H_2O)]^-$.[45,46]

https://dx.doi.org/10.1021/acs.inorgchem.0c00509
Inorg. Chem. XXXX, XXX, XXX−XXX

Table 1. Selected Bond Distances in [M(glyox)(H_2O)], M = Sc, In

distance [Å]	[Sc(glyox)(H_2O)]	[In(glyox)(H_2O)]
oxine−O	2.123(18)	2.163(6)
oxine−O	2.123(18)	2.175(5)
−COOH−O	2.090(3)	2.179(3)
water−O	2.124(3)	2.186(8)
oxine−N	2.285(2)	2.265(6)
oxine−N	2.285(2)	2.269(6)
amine−N	2.515(3)	2.546(4)

On comparing $[Sc(AAZTA)(H_2O)]^-$ with [Sc(glyox)(H_2O)], both the Sc−O and Sc−N bonds are slightly shorter in [Sc(glyox)(H_2O)] with an average Sc−O bond distance of 2.112 Å and Sc−N bond distance of 2.361 Å.[46] Meanwhile, on comparing [In(glyox)(H_2O)] and In(oxine)$_3$ structures, the average In−O (oxine) bond distances for the [In(glyox)(H_2O)] complex are slightly (0.043 Å) longer than the In(oxine)$_3$, while the average In−N (oxine) bond distances are quite similar to a negligible difference of 0.005 Å.[47] Furthermore, it is noteworthy to compare this structure with the corresponding seven coordinate In^{3+} structure of NOTA with the same N_3O_3 donor set: the average In−O bond distance for [In(glyox)(H_2O)] is shorter by 0.102 Å than for [In(NOTA)Cl], while there is a negligible difference (0.043 Å) among average In−N bond distances.[48] These structural comparisons, along with the higher pM values and thermodynamic stability constants, suggest that the preorganized H_3glyox cavity is a good match for both Sc^{3+} and In^{3+} metal ions.

Solution Thermodynamics. In the evaluation of a chelating ligand to sequester a metal ion in solution, intimate knowledge of its different ionizable protons (protonation constants) becomes crucial as the protons compete with the metal ion for the basic sites of the ligand. In this work, we have determined the six protonation constants for the six ionizable protons of H_3glyox in its fully protonated form, represented as H_6L^{3+}. Due to the ligand's lipophilic nature and lower solubility in water at millimolar concentrations, we were unable to use pH-potentiometric titrations; UV in-batch spectrophotometric titrations were employed to calculate the protonation constants, exploiting the high and different molar absorptivity for each protonated species. The titrations were done in the pH range 1.44−11.64. Seven different absorbing species were identified, showing well-defined isosbestic points, indicating different deprotonation steps of the chelator (Figures S1 and S2). The six protonation constants summarized in Table 2 were determined using the HypSpec2014 program.[49] The fully protonated ligand, H_6glyox^{3+}, shares spectral features with H_6hox^{4+} and H_8octox^{4+} due to the protonated quinoline chromophore,[32,38] having absorption bands at λ_{max} = 260 and 375 nm and an isosbestic point at λ = 247 nm (Figures S1A,B and S2). The first two acidic deprotonations of the quinoline N atoms (pK_1 = 2.66 and pK_2 = 3.33) are higher than are the analogous dissociation constants for the H_6hox^{4+} ligand (pK_1 = 0.24 and pK_2 = 0.64)—we ascribe this to the preorganized structure of the H_3glyox ligand as opposed to the open chain structure of H_2hox,[32] which facilitates intramolecular H-bonding between the O atom from the carboxylic group and the H atom bonded to the N atom of the backbone as well as H atoms from the phenolic−OH oxine arms, as shown in the crystal structure (Figure 1). Smaller spectrophotometric changes between pH 4.57 and 6.83 are due to the deprotonation of the carboxylic group in H_4glyox$^+$ (pK_3 = 5.41) to form the zwitterion H_3glyox (Figures S1A,B and S2). In this dissociation step, a higher pK_a than expected for a carboxylic acid substituent (∼pH 4) can be again explained by the H-bond stabilization in the H_4glyox$^+$ species. Between pH 6.83 and 8.32, the spectral changes are attributed to the deprotonation of the tertiary N atom of the backbone (pK_4 = 7.51; Figure S1C and D). The last two deprotonation equilibria involve dissociation of the phenolic OH protons (pK_5 = 9.70 and pK_6 = 10.66) of the quinoline moiety and the spectral changes, similar to the spectral changes for H_2hox and H_2octox^{2-},[32,38] involve disappearance of the band at 243 nm and the increase of the band at 260 nm with the isosbestic point at 249 nm and, at higher wavelengths, the decrease of the band at 308 nm with an increase of two bands at 337 and 354 nm with a new isosbestic point at 320 nm (Figures S1E,F and S2).

Table 2. Stepwise Protonation Constants (log β) and Protonation Constants (log K) of H_3glyox at 25°C

equilibrium reaction	log β	log K
$L^{3-} + H^+ \leftrightarrows HL^{2-}$	10.66 (1)[a]	10.66 (1)
$HL^{2-} + H^+ \leftrightarrows H_2L^-$	20.36 (1)[a]	9.7 (1)
$H_2L^- + H^+ \leftrightarrows H_3L$	27.87 (2)[a]	7.51 (2)
$H_3L + H^+ \leftrightarrows H_4L^+$	33.28 (1)[a]	5.41 (1)
$H_4L^+ + H^+ \leftrightarrows H_5L^{2+}$	36.61 (1)[a]	3.33 (1)
$H_5L^{2+} + H^+ \leftrightarrows H_6L^{3+}$	39.27 (1)[a]	2.66 (1)

[a]In-batch UV spectrophotometric titrations at I = 0.16 M NaCl.

Complex Formation Equilibria of H_3glyox with Sc(III), Ga(III), and In(III). Suitable radiopharmaceutical metal complexes require high thermodynamic stability and kinetic inertness to bind tightly the radionuclide and avoid any transchelation reaction by an endogenous ligand *in vivo*. Herein, the thermodynamic stabilities of H_3glyox with the trivalent metal ions Sc^{3+}, Ga^{3+}, and In^{3+} were evaluated by in-batch UV spectrophotometry. Samples of H_3glyox aqueous solutions in the presence of equimolar concentrations of each of the three different metal ions were prepared at varying pH using standardized HCl and NaOH and were allowed to reach equilibrium before measuring their UV spectra. In each of the three M^{3+}−H_3glyox experiments (M^{3+} = Sc^{3+}, Ga^{3+}, In^{3+}), the spectral changes in comparison with the electronic spectra of the ligand itself proved the formation of the metal complexes (Figures S4−S6). The analysis of the experimental data, together with the molar absorptivity of the different protonated species of H_3glyox, allowed the determination of the stability constants of the metal complexes by using HypSpec[49] (Table 3). The speciation plots for the metal complexes with Sc^{3+}, Ga^{3+}, and In^{3+} are presented in Figure 4.

Three different species were identified for each metal-H_3glyox system over the pH range 0 to 12: a monoprotonated species $[M(Hglyox)]^+$, the neutral metal complex M(glyox), and a monohydroxo species $[M(OH)(glyox)]^-$. In the case of Ga^{3+}−H_3glyox, at pH 9 the $[Ga(OH)_4]^-$ species starts to form, and as shown in the UV spectra (Figure S4F), the free ligand dominates at pH 11.

The Cram principle of preorganization states that the smaller the changes in the organization of host, guest, and solvent required for complexation, the stronger will be the binding.[51] This principle holds true here as can be seen in the

https://dx.doi.org/10.1021/acs.inorgchem.0c00509
Inorg. Chem. XXXX, XXX, XXX−XXX

Table 3. Stepwise Stability Constants (log K) of H_3glyox Complexes with Sc^{3+}, Ga^{3+}, and In^{3+} at 25°C and I = 0.16 M NaCl

equilibrium reaction	Sc^{3+}	Ga^{3+}	In^{3+}
$M^{3+} + L \leftrightarrows ML$	30.90(2)[b]	29.82(2)	38.78(1)
$ML + H^+ \leftrightarrows [MHL]^+$	2.70(2)[b]	2.49(1)	1.78(1)
$[M(OH)L]^- + H^+ \leftrightarrows ML$	10.75(2)[b]	8.99(1)	9.21(7)
pM[a]	**26.0**	**24.9**	**34.0**

[a]pM is defined as -log $[M]_{free}$ at [L] = 10 μM, [M] = 1 μM and pH = 7.4. [b]Calculated from UV and fluorometric in-batch titrations.

high log K_{ML} values for M(glyox) (M = Sc^{3+}, Ga^{3+}, and In^{3+}) which trend as In^{3+} > Sc^{3+} > Ga^{3+} and reflect the high stability of the respective metal complexes. When scrutinizing diverse chelators with different basicity and denticity for their affinity for a specific metal ion under physiologically relevant conditions, the pM value[52] (pM = $-\log[M]_{free}$ at [ligand] = 10 μM and $[M^{n+}]$ = 1 μM at pH = 7.4) tends to be more reliable for a fair comparison. To our knowledge, to date, H_3glyox has the highest pIn ever reported, higher even than that of the "gold standard" DOTA[53] (pIn = 18.8) as well as the recently reported H_4pypa[50] (pIn = 30.5) or the very similar binding moiety "oxine" (pIn = 18.7[54] for In(oxine)$_3$). In Figure 5A, the pM values for the three metal complexes with H_3glyox have been plotted showing the better fit of the preorganized H_3glyox for In^{3+}. Additionally, Figure 5B dramatically shows the strong ability of H_3glyox to complex In^{3+} at physiological pH 7.4 even compared to recent ligand candidates reported by us.[38,50] Figure 5B also shows that as the pH is raised, the metal sequestering ability in terms of pIn^{3+} depends not only on the stability constant of the metal complexes but also on the overall basicities of the ligands (Table S1). Therefore, ligands such as H_4pypa with lower overall basicity will show more complexation at lower pH and over a broader pH range, as its protons will compete less for the metal ion, whereas in the case of H_3glyox and H_4octox, complexation occurs at higher pH. The higher pIn of H_3glyox compared to that of H_4octox, even though both have similar overall basicity, resides on the higher pK_a of the In−H_4octox metal complexes, which drops the stability constant of the prevailing species at physiological pH. The high pM values of H_3glyox for Sc^{3+}, Ga^{3+}, and In^{3+} are very encouraging in terms of thermodynamic stability of the metal complexes for further *in vivo* and *in vitro* studies.

Chelation Enhanced Fluorescence Emission of H_3glyox. An additional advantage offered by the "ox" family of chelators in contrast to their picolinic acid based "pa"

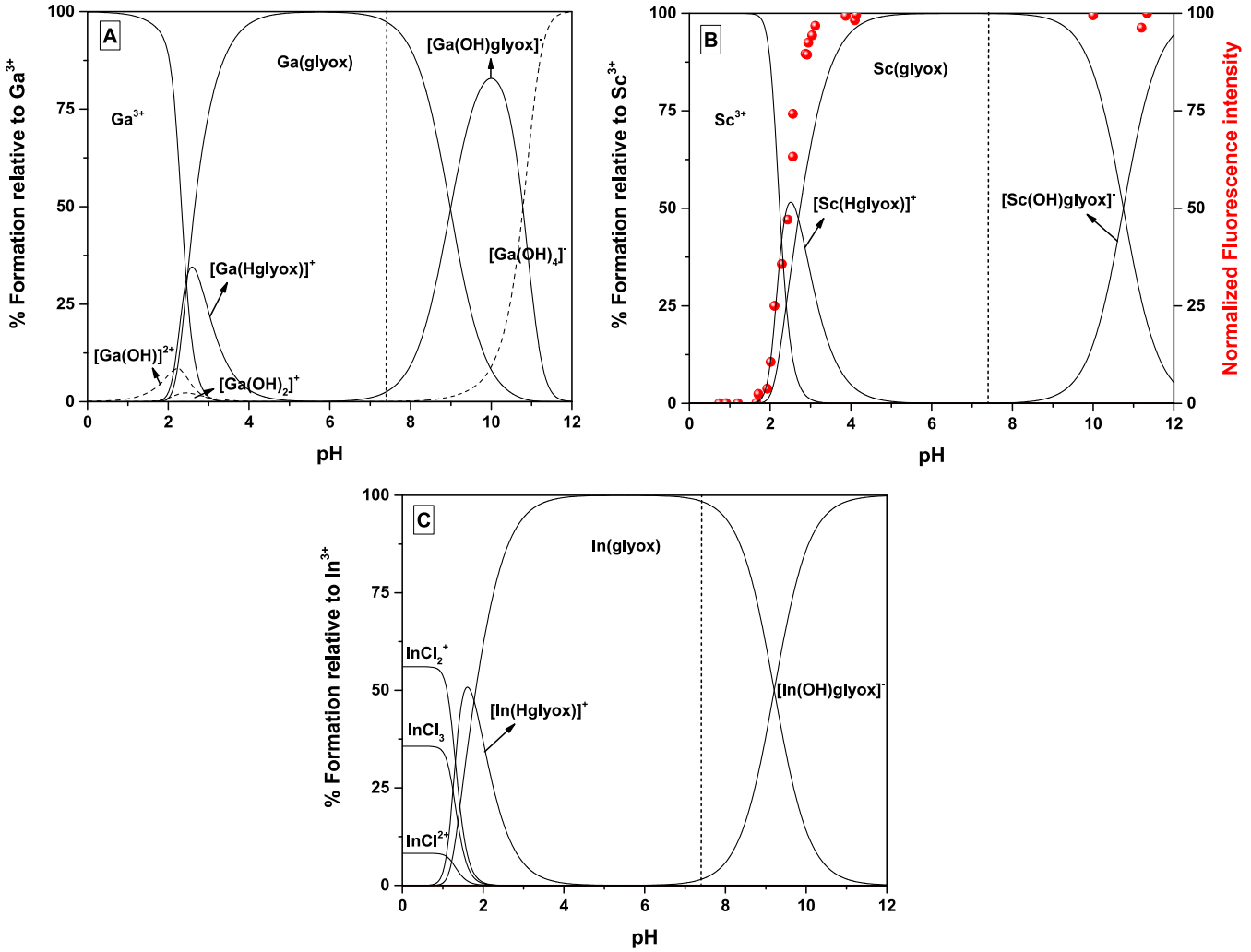

Figure 4. (A and C) Speciation of the M^{3+}−H_3glyox complexes (M^{3+}= Ga^{3+}, In^{3+}), $[M^{3+}] = [H_3glyox] = 2.48 \times 10^{-5}$ M. (B) speciation plot of Sc−H_3glyox system and normalized fluorometric titration data (red dots), $[Sc^{3+}] = [H_3glyox] = 6.51 \times 10^{-6}$ M.

https://dx.doi.org/10.1021/acs.inorgchem.0c00509
Inorg. Chem. XXXX, XXX, XXX−XXX

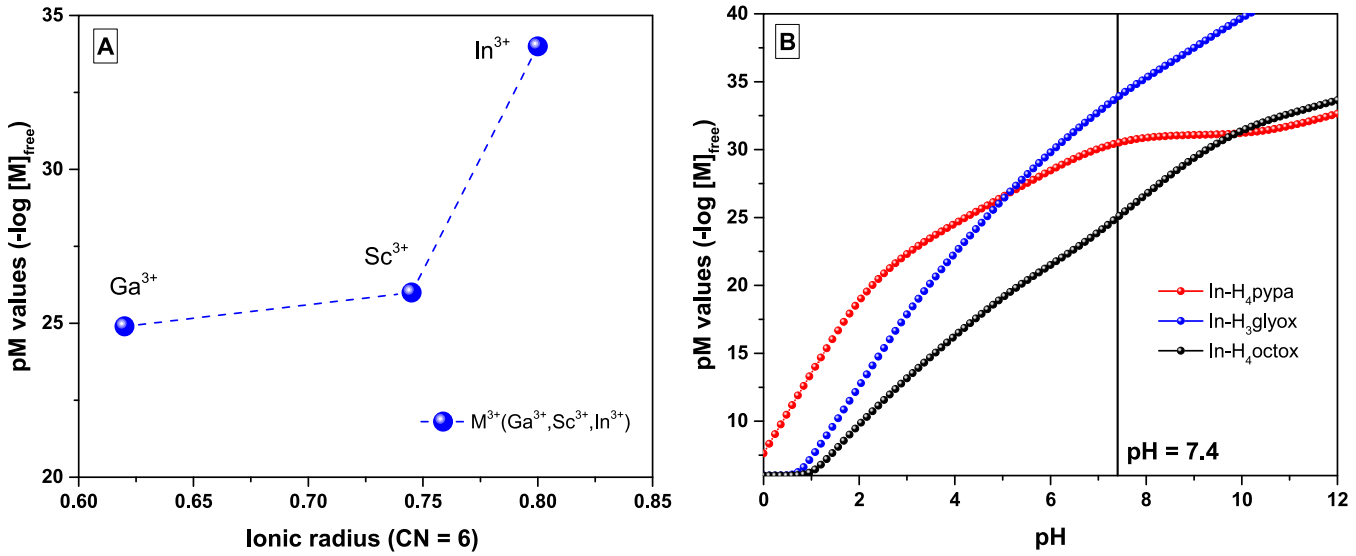

Figure 5. (A) pM values vs ionic radii[27] for M^{3+}–H_3glyox complexes (CN = 6); (B) In^{3+} scavenging ability of different ligands as the pH is raised from 0 to 12, $[In^{3+}] = 1 \times 10^{-6}$ M and [ligand] = 1×10^{-5} M. Solid line in B indicates physiological pH 7.4. Stability constants and acidity constants of ligands other than H_3glyox used for the plotting are from refs 38 and 50.

analogs is their enhanced fluorescence emission on complexation with metal ions. The neutral 8-hydroxyquinoline chromophore is usually nonfluorescent in aqueous media due to the intra- and intermolecular excited-state proton transfer along with the photoinduced electron transfer from the tertiary amine to the 8-hydroxyquinoline moiety.[55] H_3glyox showed fluorescence emission upon complexation with the Sc^{3+} trivalent ion, which was exploited to evaluate the stability constant of the metal complexes together with UV spectrophotometric titrations via in-batch fluorometric titrations as a function of pH (0.74–11.34). In Figure 4B, the fluorometric data overlap the speciation plot of the Sc^{3+}–H_3glyox system. From the analysis of the fluorometric and spectrophotometric data, the first metal complex species $[Sc(Hglyox)]^+$ would deprotonate with pK_a = 2.70 to form the neutral complex species Sc(glyox). This deprotonation can be assigned to the second phenolic–OH in the quinolone moiety, as the electronic emission spectra of the neutral species Sc(glyox) is nearly double the one of the monoprotonated $[Sc(Hglyox)]^+$ (Figure S7). This Sc^{3+} chelation enhanced fluorescence emission property could be exploited for further studies to aim imaging directed surgery in addition to the theranostic application of scandium-44 and -47 radionuclides.

Sc(glyox) and Ga(glyox) Fluorescence Cell-Imaging Studies. As discussed above, these metal complexes provide single entities that both facilitate detection of the agent using different imaging modalities (scandium-44 and gallium-68 in PET; indium-111 in SPECT; and nonradioactive Sc and Ga for optical imaging) and provide an appropriate molecule (easily accessible bifunctional chelator) that can be conjugated to the vectors (antibodies for long circulation periods or peptides for faster targeting) for targeted delivery of the drug at the site of interest. Bimodal contrast agents incorporating two different moieties (a fluorophore for optical imaging and a radioactive moiety for nuclear imaging)[56−60] or the use of nanoparticles[61] and magnetic quantum dots[62] as multimodal imaging probes are of particular focus currently. There have been however few studies on Ga^{3+} and In^{3+} complexes that comprise this bimodal imaging feature.[32,63] It is important to emphasize the surface advantages imparted by the optical probes in terms of their high spatial resolution in contrast to the nuclear imaging probes; this makes them useful for the intrasurgical identification of solid tumor tissue facilitating complete resection.[59,60,64]

Therefore, as a proof of concept, we monitored the subcellular distribution of Sc(glyox) and Ga(glyox) complexes in living HeLa cells using fluorescence microscopy (Figures 6 and S25). The HeLa cells were treated with 100 μM metal complex solution prepared in PBS for 2 h. The bright field images (Figures 6 and S25) confirmed the viability of the cells, and the accumulation of the complexes in the cytoplasm can be noted.

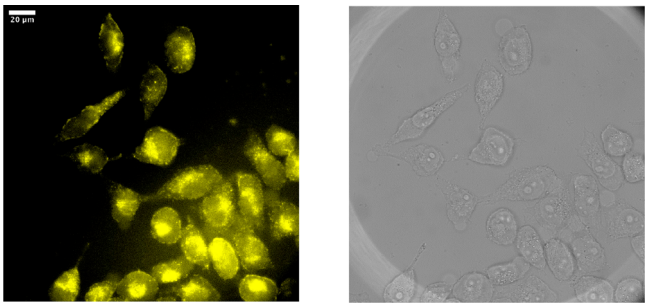

Figure 6. Live-cell fluorescence microscopy image (left) and corresponding brightfield image (right) of HeLa cells after treatment with 100 μM solution of ^{nat}Sc(glyox) in PBS for 2 h. The scale bar represents 20 μm.

pH and Concentration Dependent Gallium-68 Radiolabeling. Encouraged by the high thermodynamic stability of the Ga(glyox) complex, radiolabeling with $[^{68}Ga]GaCl_3$ was undertaken to assess the complexation kinetics and radiolabeling efficiency. The first set of experiments involved radiolabeling at three different pH values (5.5, 6.5 and 7.4; see Figure S24) using NaOAc/HOAc buffer (0.1 M, pH = 5.5, 6.5, and 7.4 respectively), followed by varying concentration of ligand solution—the results are summarized in Table 4. Quantitative radiolabeling (RCY > 95%, [L] = 10^{-5} M) was achieved at physiological pH 7.4 and room temperature within

https://dx.doi.org/10.1021/acs.inorgchem.0c00509
Inorg. Chem. XXXX, XXX, XXX–XXX

Table 4. Radiochemical Yields (RCY in %) of the Concentration Dependent Experiments for the Gallium-68, Indium-111, and Scandium-44 Complexes of H_3glyox (n = 3)

[ligand] (M)	^{68}Ga RCY (%)[a]	^{111}In RCY (%)[b]	^{44}Sc RCY (%)[b]
10^{-4}	>95	100	100
10^{-5}	>95	100	100
10^{-6}	90	100	100
10^{-7}	80	100	ND
10^{-8}	45	100	ND
10^{-9}	5	15	ND

[a]Room temperature, 0.1 M NaOAc/HOAc, pH = 7.4, 5 min. [b]Room temperature, 0.1 M NaOAc/HOAc, pH= 7, 15 min.

5 min with the apparent molar activity of 750 MBq/μmol (Table 4). The radiochemical yields were assayed by radio-iTLC (stationary phase- aluminum backed silica gel TLC plate; mobile phase = 0.1 M sodium citrate; cf. Figures S19 and S20). The [^{68}Ga]Ga(glyox) complex remained at the origin (R_f < 0.1) while the "free" radiometal ion migrated up to the solvent front (R_f > 0.5). These RCY data were confirmed by radio-HPLC with well-resolved peaks (t_R = 3 min for the [^{68}Ga]Ga(glyox) complex, t_R = 15 min for "free" [^{68}Ga]Ga^{3+}, cf. Figures S21 and S22). Distribution ratios log $D_{o/w}$ of the radiolabeled complex were determined in a two-phase extraction system consisting of 1-octanol/aqueous buffer (pH = 7.2, 7.4, 7.6) in order to get information about the hydrophilic character of this complex. The log $D_{7.2}$, log $D_{7.4}$, and log $D_{7.6}$ were measured to be −0.10, −0.22, and −0.33, respectively. As expected, the measurements showed that [^{68}Ga]Ga(glyox), being a charge neutral complex, is slightly more lipophilic than the corresponding charged gallium-68 complexes of H_2hox (−0.47), DOTAGA-cNGR (−3.50), NODAGA-cNGR (−3.30), and HBED-CC-cNGR (−2.80).[65] There are studies that suggest that increased lipophilic character of the tracer leads to higher tumor uptake, along with the longer retention times, beneficial in the sensitive detection of the smaller tumor masses as well as for radiotherapy.[30,66,67]

[^{68}Ga]Ga(glyox) Complex Stability in Human Serum. Although the high thermodynamic stability of the metal complexes is desirable, kinetic inertness *in vivo* plays a determining role for using these complexes for application in nuclear medicine. An additional non-negligible factor while working with ^{68}Ga-based chelators is the affinity of the iron-sequestering protein transferrin (log K_{ML} = 19.75), which is capable of transchelating weakly bound Ga^{3+} due to the similarity between the charge-to-size ratios of Ga^{3+} and Fe^{3+}.[68] Therefore, the stability of the [^{68}Ga]Ga(glyox) complex in human serum was quantitatively evaluated using a standard gel electrophoresis technique.[69] Shown in Figure 7 is the depiction of the nonreducing SDS polyacrylamide gel obtained by the serum stability assays. A prominent protein band in the size range of ∼70 kDa which corresponds to radioactive transferrin is visible in the autoradiographic scan. Lanes 1, 2, and 3 depict the triplicates for the assays containing the [^{68}Ga]Ga(glyox) complex, while lane 4 depicts the control assay with [^{68}Ga]$GaCl_3$ (absence of chelator) in human serum. The altered blackening intensities of the transferrin band originate from the loss of ^{68}Ga from the chelate upon incubation with human serum (pH 7.4, 37 °C) for 1 h. Remarkably, the gallium−glyox complex is stable under these most relevant conditions with less than 2% transchelation (calculated using equations described in the Experimental Section) and exhibits great potential for its development as a ^{68}Ga-based radiopharmaceutical.

Radiolabeling and Stability of [^{111}In]In(glyox) in Human Serum. Radiolabeling experiments of [^{111}In]$InCl_3$ as a function of H_3glyox ligand concentration were performed to determine the efficiency of H_3glyox to sequester the SPECT radionuclide ^{111}In ($t_{1/2}$ = 2.8 d), and these studies show excellent quantitative radiolabeling efficacy (>99%, see Table 4) with $^{111}InCl_3$ within 15 min at room temperature and neutral pH (0.1 M NaOAc/HOAc buffer, pH 7), with ligand concentration as low as 10^{-8} M and a high apparent molar activity of 650 MBq/nmol. The radiochemical yields were assayed by radio-iTLC, integrating the area under the peaks observed ([^{111}In]In(glyox), R_f < 0.1; [^{111}In]InEDTA, R_f > 0.7; Figure S16) when developed with EDTA solution (0.1 M, pH 7), consistent with the well-resolved sharp peaks observed in HPLC radio-traces (Figure S17) for the "free" ^{111}In (t_R = 4.9 min) and [^{111}In]In(glyox) (t_R = 12.2 min). As discussed earlier there are several endogenous ligands (transferrin, albumin, other metalloproteins) present in the human body with a variety of binding sites that can displace the radiometal ion and lead to undesired transchelation *in vivo*. As for gallium, transferrin has been well-documented for its substantial

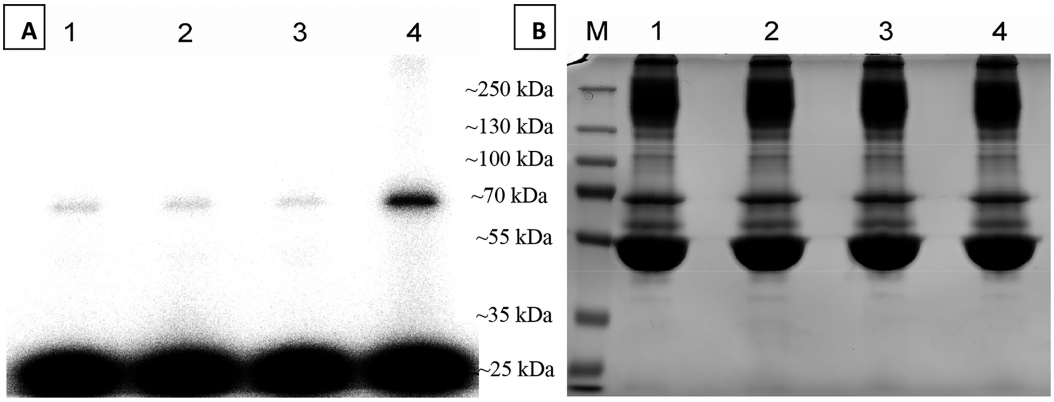

Figure 7. Analysis of ^{68}Ga incorporation into human serum proteins. Autoradiography (a) and colloidal Coomassie stained 10% SDS-polyacrylamide gel (b) showing ^{68}Ga-labeled bands of human serum proteins: lanes 1−3, ^{68}Ga-labeled H_3glyox chelator (triplicate); lane 4, [^{68}Ga]$GaCl_3$ (control sample with no chelator).

https://dx.doi.org/10.1021/acs.inorgchem.0c00509
Inorg. Chem. XXXX, XXX, XXX−XXX

binding capacity for In^{3+} (log K_{1M} = 18.30, log K_{2M} = 16.44)[70] given that only 30% of the protein is saturated with iron under normal serum conditions. Hence, it is very important that the metal complex is stable under normal serum conditions; the [^{111}In]In(glyox) complex was incubated with an excess of human serum (37 °C, pH 7.4) and the stability of the [^{111}In]In(glyox) was monitored every day for seven consecutive days using iTLC (Figure S23). The results showed that the complex was exceptionally stable with <1% transchelation over 7 days comparable to the 5 days reported for [^{111}In][In(pypa)]$^-$;[50] this is in contrast to the *in vivo* stability of the other macrocyclic as well as nonmacrocyclic chelators developed for ^{111}In-based radiopharmaceuticals (see Table 5).

Table 5. Human Serum Stability Challenge Data Performed at 37°C (n = 2), with Stability Shown as Percentage of Intact Indium-111 Complex (RCY in %)

complex	24 h stability	5 day stability	7 day stability
[^{111}In]In(glyox)	<99	<99	<99
[^{111}In][In(bispox^2)]$^{+a}$	94.6 ± 0.4	89.4 ± 0.6	NA
[^{111}In][In(pypa)]$^{-b}$	<99	<99	NA
[^{111}In][In(octox)]$^{-c}$	91.4 ± 0.6	83.6 ± 1.4	NA
[^{111}In]In(octapa)]$^{-d}$	92.3 ± 0.04	NA	NA
[^{111}In][In(DOTA)]$^{-d}$	89.4 ± 2.2	NA	NA
[^{111}In][In(DTPA)]$^{2-d}$	88.3 ± 2.2	<60	NA

[a]From ref 71. [b]From ref 50. [c]From ref 38. [d]From ref 53.

Scandium-44 Radiolabeling. Aided by the high thermodynamic stability of Sc(glyox) reflected in log K_{ML}= 32 and pM = 26 (*vide supra*), preliminary labeling experiments were performed with [^{44}Sc]$ScCl_3$. The experiments demonstrated that H_3glyox ([L] = 10^{-6} M) complexes scandium-44 (~0.5 MBq per reaction, n = 3) quantitatively (>99%) within 10 min under ambient conditions (0.1 M NaOAc/HOAc, pH = 7, room temperature). The radiolabeling yields were assayed by radio-iTLC (aluminum-backed silica gel) plates using 0.1 M EDTA (pH 7) as the mobile phase. [^{44}Sc]Sc(glyox) remained at the baseline with R_f < 0.1 while "free" [^{44}Sc]Sc^{3+} migrates up the plate with R_f > 0.8 (Figure S18). It is worth mentioning that some of the previously reported chelators (H_4pypa,[16] AAZTA,[46] H_3mpatcn[17]) for Sc^{3+} incorporate carboxylic acid and picolinic acid moieties for faster chelation, which optimizes radiolabeling at more acidic pH, but the oxine arms in H_3glyox facilitate radiolabeling at slightly more basic physiological pH (~7.4), advantageous when the BFC is conjugated to an antibody first and subsequently radiolabeled—the procedure when working with shorter-lived radioisotopes. Although, both H_4pypa (pSc = 27.1)[16] and H_3glyox (pSc = 26.0) have similar affinities for Sc^{3+}, [Sc(pypa)]$^-$ exists in two isomeric forms in solution at room temperature, while Sc(glyox) exists as a single species both in the solid state as well as in solution.

CONCLUSIONS

The hexadentate chelator H_3glyox showed its great affinity for smaller trivalent metal ions such as those of scandium-44, gallium-68, and indium-111, reflected by their high pM values in the order pIn (34.0) > pSc (26.0) > pGa (24.9) and the quantitative radiolabeling yields achieved under ambient conditions (RT, 10 min, pH 7). The increased rigidity and differences in basicity of the oxine arms with respect to picolinic acid arms in H_3dpaa resulted in the increased stability of the [^{68}Ga]Ga(glyox) complex against transchelation (<2%) in human serum, better than that of the "gold standard" [^{67}Ga][Ga(DOTA)]$^-$ after 1 h of incubation; Ga(glyox) is also more lipophilic.[37] The same chelator to complex with different metal ions provides a chemically reproducible tool to compare the pharmacokinetics of different metal ions in the body and more importantly to use the same scaffold for imaging and/or for therapy depending on the radionuclidic emission. Moreover, quantitative radiolabeling of ^{111}In with ligand concentrations as low as 10 nM under ambient conditions (RT, pH 7) is remarkable with a high apparent molar activity of 650 MBq/nmol, and it precludes the need for any purification postlabeling. [^{111}In]In(glyox) is extremely stable even after 7 days of incubation in human serum. In summary, all these attributes of H_3glyox along with the facile and inexpensive synthesis of the bifunctional derivatives by incorporating other amino acids in place of the glycine residue display potential for development as versatile tracers in nuclear and fluorescence imaging. A bifunctional chelating analogue, using p-NO_2 phenylalanine amino acid as an anchor connection, is currently under investigation, and further detailed radiolabeling with ^{44}Sc and comparison of the biodistribution studies of the bifunctional derivative with scandium-44 and gallium-68 PET imaging will be reported.

EXPERIMENTAL SECTION

Materials and Methods. All solvents and reagents were purchased from commercial suppliers (Sigma-Aldrich, TCI America, Fischer Scientific, Alfa Aesar) and were used as received. Reactions were monitored by TLC (MERCK Kieselgel 60 F254, aluminum sheet). Flash chromatography was performed using Silicaflash F60 silica gel (40−63 μM particle size), Redisep Rf HP silica columns, and a Combiflash Rf column machine. Water used was ultrapure (18.2 MΩ cm^{-1} at 25 °C, Milli-Q, Millipore, Billerica, MA).

^{1}H and ^{13}C NMR spectroscopies were performed on either Bruker Advance 300 or Bruker AV III HD 400 MHz spectrometers. Chemical shifts (δ) are quoted in ppm relative to residual solvent peaks as appropriate. Coupling constants (J) are provided in Hertz (Hz). ^{1}H NMR signals were designated as follows: s (singlet), d (doublet), t (triplet), q (quartet), quin (quintet), sxt (sextet), spt (septet), m (multiplet), or a combination of these, with br representing a broad signal. Low resolution ESI-MS was performed on a Waters 2965 HPLC- MS with the sample prepared in methanol or ACN. Results are labeled with m/z (abundance percentage) values − $[M + X]^{\mp}$. High resolution ESI-MS was performed on a Waters/Micromass LCT TOF-MS with the sample prepared in methanol. Results are labeled with m/z (abundance percentage) values. Semipreparative reverse phase high-performance liquid chromatography (HPLC) for H_3glyox and In(glyox) was performed on a Phenomenex 16 synergi hydro-RP 80 Å, 250 × 21.2 mm column connected to a Waters 600 controller, a Waters 2487 dual wavelength absorbance detector, and a Waters delta 600 pump. The HPLC solvents were (A) H_2O containing 0.1% trifluoroacetic acid (TFA) and (B) CH_3CN containing 0.1% TFA. Silica gel impregnated TLC plates (MERCK Kieselgel 60 F254, aluminum sheet) were used to analyze gallium-68, scandium-44, and indium-111 radiolabeling reaction progress and the complex stability; human serum stability tests were counted on a BioScan System 200 imaging scanner equipped with a BioScan Autochanger 1000.

Synthesis and Characterization. *8-Hydroxyquinoline-2-aldehyde (1).* 2-Methyl-8-hydroxyquinoline (5.00 g, 30 mmol) was dissolved in 1,4-dioxane (50 mL) and added dropwise to a solution of selenium oxide (5.02 g, 45 mmol) in 1,4-dioxane (150 mL) in a 250 mL round-bottom flask and left to stir overnight at 80 °C. The reaction mixture was then cooled and filtered through Celite, and the filtrate was concentrated under reduced pressure to yield dark orange product. The crude product was purified by silica chromatography (hexane/ethyl acetate, 9:1−1:1) to yield pure yellow needle-like crystals (4.40 g, 25 mmol, 82%, R_f = 0.70 in 10% EtOAc in hexane).

https://dx.doi.org/10.1021/acs.inorgchem.0c00509
Inorg. Chem. XXXX, XXX, XXX−XXX

^{1}H NMR (300 MHz, $CDCl_3$, RT): δ 10.23 (s, 1H), 8.32 (d, J = 8.5, 1H), 8.17 (s, 1H), 8.08 (d, J = 8.5 Hz, 1H), 7.63 (t, J = 8.5 Hz, 1H), 7.45 (dd, J = 8.4 Hz, 1H), 7.30 (d, J = 7.6 Hz, 1H). ^{13}C NMR (75 MHz, $CDCl_3$, RT): δ 192.8, 153.1, 150.3, 137.9, 137.6, 131.1, 130.5, 118.2, 118.1, 111.4. LR-ESI-MS: $[C_{10}H_7NO_2 + Na]^+$ calcd., 196.0; $[M + Na]^+$ found, 196.3.

*Ethyl Bis((8-hydroxyquinolin-2-yl)methyl)glycinate (**2**).* Compound **1** (1 g, 5.7 mmol, 2.1 equiv) was dissolved in 50 mL of 1,2-dichloroethane, and to this solution was added glycine ethyl ester, HCl (0.8 g, 2.7 mmol, 1 equiv), and $NaBH(OAc)_3$ (2.8 g, 13.5 mmol, 5 equiv). The mixture was refluxed overnight at 50 °C, then quenched with saturated aqueous Na_2CO_3 (20 mL) and extracted with dichloromethane (3 × 20 mL). The combined organic layers were dried over anhydrous $MgSO_4$. The solvent was removed under a vacuum to give crude product **2**, which was then purified by column chromatography (eluted with a gradient of 100% hexane to 100% ethyl acetate) to afford **2** as an off-white solid (0.7 g, 1.6 mmol, 61%, R_f = 0.50 in 20% EtOAc in hexane). ^{1}H NMR (300 MHz, $CDCl_3$, RT): δ 8.11 (d, J = 8.5 Hz, 2H), 7.72 (d, J = 8.5 Hz, 2H), 7.41 (m, 2H), 7.31 (d, J = 8.2 Hz, 2H), 7.17 (d, J = 7.5 Hz, 2H), 4.19 (m, 6H), 2.03 (s, 2H), 1.27 (t, J = 7.1 Hz, 3H). ^{13}C NMR (75 MHz, $CDCl_3$, RT): δ 171.3, 160.6, 157.1, 145.3, 140.8, 136.5, 136.4, 134.1, 128.9, 128.8, 127.0, 125.8, 122.9, 122.2, 60.7, 60.3, 55.4, 14.4.

*Bis((8-hydroxyquinolin-2-yl)methyl)glycine, H_3glyox (**3**).* A portion of **2** was dissolved in HCl (10 mL, 6 M) and refluxed overnight. The solution was cooled, and the solvent was evaporated under reduced pressure to give a yellow colored solid product **3** (0.5 g, 1.3 mmol, 76%). ^{1}H NMR (300 MHz, RT, D_2O): δ 8.54 (d, J = 7.7 Hz, 2H), 7.72 (d, J = 7.9 Hz, 2H), 7.45 (t, J = 7.2 Hz, 2H), 7.31 (d, J = 7.6 Hz, 2H), 7.15 (d, J = 6.7, 2H), 4.52 (s, 4H), 4.04 (s, 2H). ^{13}C NMR (75 MHz, RT, D_2O): δ 176.1, 155.1, 150.4, 146.9, 146.6, 130.9, 128.8, 128.4, 122.3, 119.2, 117.0, 58.5, 57.3. HR-ESI-MS calcd for $C_{22}H_{19}N_3O_4$: 389.1400. Found: 390.1451 $[M + H]^+$. Anal. calcd. for $[H_3glyox{\cdot}2.8\ HCl{\cdot}1.3\ CH_3OH)]$: C, 52.49; H, 5.1; N, 7.88. Found: C, 52.48; H, 5.11; N, 7.93.

In(glyox). A portion of H_3glyox (10 mg, 0.02 mmol) was dissolved in 1 mL of distilled water, and $In(ClO_4)_3$ (11.7 mg, 0.02 mmol) was added to it. Using 0.1 M NaOH, the pH was adjusted to ∼7, and the solution was left to stir for 1 h. The solvent was evaporated under reduced pressure to give yellow colored metal complex as a hydrate. HR-ESI-MS calcd for $C_{22}H_{16}InN_3NaO_4$: 524.0077. Found: 524.0076 $[M + Na]^+$.

Ga(glyox). To a solution of H_3glyox (10 mg, 0.02 mmol) dissolved in 1 mL of distilled water was added $Ga(NO_3)_3$ (7.23 mg, 0.02 mmol), and the pH was adjusted to ∼7 using 0.1 M NaOH. The solution was left to stir overnight, and the solvent was evaporated under reduced pressure to give a pale yellow colored metal complex as a hydrate. ^{1}H NMR (300 MHz, RT, D_2O): δ 7.69 (d, J = 8.4 Hz, 2H), 7.11 (t, J = 7.8 Hz, 2H), 7.05 (d, J = 8.4 Hz, 2H), 6.71 (d, J = 8.6 Hz, 2H), 6.59 (d, J = 7.7 Hz, 2H), 3.76 (s, 4H), 3.05 (s, 2H). ^{13}C NMR (75 MHz, $CDCl_3$, RT): δ 179.8, 164.1, 155.4, 143.0, 136.9, 129.4, 128.5, 121.7, 114.0, 111.3, 60.7, 59.3. HR-ESI-Ms calcd for $C_{22}H_{16}GaN_3NaO_4$: 478.0294. Found: 478.0296 $[M + Na]^+$.

Sc(glyox). H_3glyox (10 mg, 0.02 mmol) was dissolved in 1 mL of distilled water in a scintillation vial, and $ScCl_3$ (5.18 mg, 0.02 mmol) was added, followed by pH adjustment to ∼6 using 0.1 M NaOH. The solution was left to stir for 1 h, and formation of the metal complex was confirmed using LR-ESI MS as well as fluorescence under a UV lamp. HR-ESI-MS calcd for $C_{22}H_{17}N_3O_4Sc$: 432.0778. Found: 432.0777 $[M + H]^+$.

Solution Thermodynamics. Protonation constants and metal stability constants were calculated from UV spectrophotometric titration data obtained using a Cary 60 UV−vis spectrophotometer in the spectral range of 200−450 nm. The path length was 1 cm for all samples. Individual samples (5 mL) containing the ligand (H_3glyox, $[L] = 2.5 \times 10^{-5}$ M) and the corresponding metal complexes (M = Ga^{3+}, In^{3+}; $[ML] = 2.5 \times 10^{-5}$ M) were prepared in pure water by adjusting the pH using standardized HCl or NaOH solutions, and NaCl was added to maintain a constant 0.16 M ionic strength over the pH range ∼0.64−11.64. In the complex formation equilibria studies with Sc^{3+}, two in-batch methods were used to determine the stability constants: UV spectrophotometric and fluorometric titrations. The metal−ligand concentration ($[ML] = 6.51 \times 10^{-6}$ M) was lower than that in the other experiments due to the lower solubility of the neutral Sc(glyox) species. A Ross combination pH electrode was calibrated for hydrogen ion concentration using HCl as described before,[37] and the results were analyzed by the Gran[72] procedure. The pH of the samples containing ligand and the metal−ligand complex was measured between the pH range of 1.8 and 11.5. For the most acidic samples, the equilibrium H^+ concentration was calculated from solution stoichiometry and was not measured with the glass electrode. For the ligand protonation equilibria study, the samples were left for 2 min to achieve equilibrium before measuring the pH and the UV absorption spectrum. For the samples containing the metal complexes, the measurements were performed only when equilibrium was achieved. The protonation constants of H_3glyox and the metal-complex stability constants were calculated from the experimental data using the HypSpec2014[49] program. Proton dissociation constants corresponding to hydrolysis of Ga^{3+}, In^{3+}, and Sc^{3+} aqueous ions included in the calculations were taken from Baes and Mesmer.[73] The species formed in the studied systems are characterized by the general equilibrium: pM + qH + rL = MpHqLr (charges omitted). For convention, a complex containing a metal ion M, proton H, and ligand L has the general formula MpHqLr. The stoichiometric indices p might also be 0 in the case of ligand protonation equilibria, and negative values of q refer to proton removal or hydroxide ion addition during formation of the complex. The overall equilibrium constant for the formation of the complexes MpHqLr from its components is designated as log β. Stepwise equilibrium constants log K correspond to the difference in log units between the overall constants of sequentially protonated (or hydroxide) species. pM value is defined as $-\log[M^{n+}]_{free}$ calculated at specific conditions ($[M^{n+}] = 10$ μM, $[L^{x-}] = 1$ μM, pH 7.4).[52]

Radiolabeling Experiments. A stock solution of the ligand, H_3glyox, was prepared (7.64×10^{-5} M) in MQ water. For concentration dependent experiments, different ligand solutions were prepared by diluting the stock solution using a corresponding buffer solution such that the total volume per reaction was 500 μL after the addition of $[^{111}In]InCl_3$, $[^{68}Ga]GaCl_3$, or $[^{44}Sc]ScCl_3$.

Concentration Dependent $[^{111}In]In(glyox) Radiolabeling and Complex Stability Studies in Human Serum. All labeling reactions were done over a time period of 15 min at room temperature and pH 7. The total volume of the reaction mixture was 500 μL after the addition of ∼900 kBq of $[^{111}In]InCl_3$ using 0.1 M NaOAc/HOAc buffer (pH = 7) and an appropriate amount of the ligand stock solution. The RCYs were obtained by analyzing the reaction mixture by spotting an aliquot on an aluminum-backed silica TLC plate and developed using a 10 mM EDTA solution (pH = 7) as a mobile phase. The $[^{111}In]In(glyox)$ complex stays at the baseline (R_f = 0) while the uncomplexed $[^{111}In]In^{3+}$ migrates up the plate as the EDTA complex (R_f > 0.7). Developed plates were counted immediately, and radiolabeling yields were calculated by integrating the peaks in the radio-chromatogram, consistent with the well-separated radio peaks of the "free" $[^{111}In]In^{3+}$ metal ion and the $[^{111}In]In(glyox)$ complex on the HPLC radiotraces (t_R = 4.9 min for "free" ^{111}In and 12.2 min for $[^{111}In]In(glyox)$ complex). For the human serum challenge, 500 μL of human serum was added to a quantitative radiolabeled complex solution (500 μL). The mixture was then incubated at 37 °C. An aliquot of the reaction mixture was spotted on silica plates at desired time points to determine the amount of intact complex (RCY%).

pH and Concentration Dependent $[^{68}Ga]Ga(glyox) Radiolabeling Procedure. All pH dependent radiolabeling reactions were done at room temperature over a 5 min period, and the total volume of the reaction mixture was kept to 500 μL after addition of 5 MBq $[^{68}Ga]GaCl_3$ and the corresponding NaOAc/HOAc buffer (0.1 M, pH = 5.5, 6.5, 7.3) such that the final ligand concentration was 10^{-4} M. For the concentration dependent radiolabeling, reaction solutions with varying ligand concentrations (10^{-4} M to 10^{-9} M) were prepared by diluting the stock solution of the ligand (∼10^{-3} M) using 0.1 M

https://dx.doi.org/10.1021/acs.inorgchem.0c00509
Inorg. Chem. XXXX, XXX, XXX−XXX

NaOAc/HOAc (pH = 7.3) and addition of 5 MBq of [^{68}Ga]$GaCl_3$. Radiochemical yields were obtained by analyzing the reaction mixture using aluminum-backed silica TLC plates as a stationary phase and 0.1 M sodium citrate as the mobile phase. The [^{68}Ga]Ga(glyox) complex stayed at the baseline of the TLC plate (R_f < 0.1), while the "free" ^{68}Ga migrated to the solvent font as the [^{68}Ga]Ga−citrate complex (R_f > 0.5). The radiochemical purity was analyzed using HPLC and ZIC-HILIC columns by running a gradient of 0−20% A for 5 min and 20−90% A for 10−20 min (A: 0.1 M NH_4OAc, pH = 5.6; B: ACN). The retention time for [^{68}Ga]Ga(glyox) is 3 min and for "free" ^{68}Ga is 15 min.

[^{68}Ga]Ga(glyox) Complex Stability Studies in Human Serum. Aliquots of human serum were thawed on ice and filtered using syringe filters with a pore size of 0.2 μm. After mixing the filtered serum (220 μL) with 1 M HEPES/NaOH buffer (pH 7.4, 45 μL), 105 μL of [^{68}Ga]Ga(glyox) (~16 nmol) was added, and the reaction mixture was incubated for 1 h at 37 °C. The reaction mixture was then mixed with 6× Laemmli sample buffer (74 μL). The mixtures were separated using nonreducing SDS-polyacrylamide gel electrophoresis (SDS- PAGE) with acrylamide concentrations of 5% in the stacking and 10% in the resolving gel, respectively. Each sample (2 μL) was loaded into each well of the gels. The SDS-PAGE was run at room temperature and 80 V until the dye front reached the resolving gel, and then potential was increased to 200 V. After electrophoresis, the gel was washed for 1 min in MQ water and was exposed to a high resolution phosphor imaging plate. The exposed plates were scanned with an Amersham Typhoon 5 Scanner, and the gels were stained with PageBlue protein staining solution according to the manufacturer's instructions. Transchelation was quantitatively determined using the following equations:

$$X_{\text{reference}} = \text{integral/activity}$$

$$Y_{\text{sample}} = \text{integral/activity transchelation [\%of control]} = (Y_{\text{sample}}/X_{\text{reference}}) \times 100$$

Determination of Distribution Ratio log $D_{o/w}$ at 25 ± 1 °C. Log D of [^{68}Ga]Ga(glyox) was determined using 1-octanol/buffer mixtures. The experiments were performed with a 100 μm solution of H_3glyox dissolved in aqueous buffer solutions. Aqueous phases consisted of 440 mL of 50 μm 4-(2-hydroxyethyl)-1-piperazine ethanesulfonic acid (HEPES)-NaOH buffer (pH 7.2, 7.4, 7.6) and 60 μL of [^{68}Ga]$GaCl_3$ solution (5 MBq). The distribution experiments were carried out at 25 ± 1 °C in microcentrifuge tubes (2 cm^3) with mechanical shaking for 30 min. The phase ratio $V_{(1\text{-octanol})}/V_{(aq)}$ was 1:1 (0.5 mL each). Full complexation was checked by radio-TLC, which gave no evidence of free ^{68}Ga in the aqueous phase. All samples were centrifuged and the phases then separated. The gallium(III) complex concentration in both phases was determined radiometrically using γ-radiation (^{68}Ga, NaI(Tl) scintillation counter automatic gamma counter 1480, Wizard 3″, Perkin−Elmer). The results are the average values of two independent experiments.

Solid State X-ray Analysis. Single yellow needle-shaped crystals of $C_{22}H_{19}N_3O_4$, H_3glyox, were obtained by slow evaporation of a solution of H_3glyox dissolved in water and acetonitrile (30:70). A suitable crystal of 0.22 × 0.20 × 0.05 mm^3 was selected and mounted on a Mylar loop on a Bruker APEX II area detector diffractometer. The crystal was kept at a steady T = 90 K during data collection. The structure was solved with the XT[74] structure solution program using the Intrinsic Phasing solution method and Olex2[75] as the graphical interface. The model was refined with version 2018/1 of ShelXL[74] using least-squares minimization.

Single yellow needle-shaped crystals of $C_{22}H_{20}N_3O_6Sc$, [Sc(glyox)-H_2O], were obtained by slow evaporation of an aqueous solution of Sc(glyox). A suitable crystal of 0.23 × 0.18 × 0.07 mm^3 was selected and mounted on a support on a Bruker APEX-II CCD diffractometer. The crystal was kept at a steady T = 90 K during data collection. The structure was solved with the ShelXT[74] structure solution program using the intrinsic phasing solution method and Olex2[75] as the graphical interface. The model was refined with version 2018/1 of ShelXL[74] using least-squares minimization.

Single colorless crystals of $C_{22}H_{20}InN_3O_6$, [In(glyox)H_2O], were obtained by slow evaporation of an aqueous solution of In(glyox). A suitable crystal of 0.79 × 0.19 × 0.17 mm^3 was selected and mounted on a suitable support on a Bruker APEX II area detector diffractometer. The crystal was kept at a steady T = 90.0 K during data collection. Using Olex2,[75] the structure was solved with the SIR2004[76] structure solution program using direct methods and refined with the XH[74] refinement package using CGLS minimization.

Fluorescence Imaging. Hela cells were purchased from the American Type Culture Collection (ATCC). Cells were grown in Eagle's Minimal Essential Medium (MEM) supplemented with heat-inactivated 10% fetal bovine serum, 1 mM sodium pyruvate, 4 mM L-glutamine, and 1% nonessential amino acids in a humidified incubator at 37 °C and 5% CO_2. Cells were seeded in two-well culture slips 24 h prior to treatment. The [Ga(glyox)] and [Sc(glyox)] working solution for fluorescence microscopy was prepared from a PBS stock solution. No precipitation of the compound was observed in the working solution under this condition. Cells were exposed to 100 μM [Ga(glyox)] or [Sc(glyox)] for 24 h and washed with phosphate buffered saline (PBS) thrice before being fixed with aldehyde, and imaging was done using a Olympus IX83 Inverted fluorescence microscope and Cell-F fluorescence imaging software (Olympus).

■ ASSOCIATED CONTENT

Supporting Information

The Supporting Information is available free of charge at https://pubs.acs.org/doi/10.1021/acs.inorgchem.0c00509.

Detailed information on ^{1}H NMR and ^{13}C NMR spectra of compounds, solution studies, X-ray crystallography data, HPLC radio-traces, and detailed i-TLC radio-chromatographs (PDF)

Accession Codes

CCDC 1983452−1983453 and 1983463 contain the supplementary crystallographic data for this paper. These data can be obtained free of charge via www.ccdc.cam.ac.uk/data_request/cif, or by emailing data_request@ccdc.cam.ac.uk, or by contacting The Cambridge Crystallographic Data Centre, 12 Union Road, Cambridge CB2 1EZ, UK; fax: +44 1223 336033.

■ AUTHOR INFORMATION

Corresponding Author

Chris Orvig − *Medicinal Inorganic Chemistry Group, Department of Chemistry, University of British Columbia, Vancouver, British Columbia V6T 1Z1, Canada;* orcid.org/0000-0002-2830-5493; Email: orvig@chem.ubc.ca

Authors

Neha Choudhary − *Medicinal Inorganic Chemistry Group, Department of Chemistry, University of British Columbia, Vancouver, British Columbia V6T 1Z1, Canada; Life Sciences Division, TRIUMF, Vancouver, British Columbia V6T 2A3, Canada*

María de Guadalupe Jaraquemada-Peláez − *Medicinal Inorganic Chemistry Group, Department of Chemistry, University of British Columbia, Vancouver, British Columbia V6T 1Z1, Canada;* orcid.org/0000-0002-6204-707X

Kristof Zarschler − *Life Sciences Division, TRIUMF, Vancouver, British Columbia V6T 2A3, Canada;* orcid.org/0000-0002-7571-4732

Xiaozhu Wang − *Medicinal Inorganic Chemistry Group, Department of Chemistry, University of British Columbia, Vancouver, British Columbia V6T 1Z1, Canada;* orcid.org/0000-0002-5882-0066

https://dx.doi.org/10.1021/acs.inorgchem.0c00509
Inorg. Chem. XXXX, XXX, XXX−XXX

Valery Radchenko − *Life Sciences Division, TRIUMF, Vancouver, British Columbia V6T 2A3, Canada; Department of Chemistry, University of British Columbia, Vancouver, British Columbia V6T 1Z1, Canada*

Manja Kubeil − *Institute of Radiopharmaceutical Cancer Research, Helmholtz-Zentrum Dresden-Rossendorf, D-01328 Dresden, Germany;* orcid.org/0000-0001-8857-5922

Holger Stephan − *Institute of Radiopharmaceutical Cancer Research, Helmholtz-Zentrum Dresden-Rossendorf, D-01328 Dresden, Germany;* orcid.org/0000-0002-2972-2803

Complete contact information is available at: https://pubs.acs.org/10.1021/acs.inorgchem.0c00509

Notes

The authors declare no competing financial interest.

■ ACKNOWLEDGMENTS

We gratefully acknowledge both the Canadian Institutes for Health Research (CIHR) and the Natural Sciences and Engineering Research Council (NSERC) for grant support, NSERC for an IsoSiM CREATE at TRIUMF studentship (N.C.), and MITACS for a Globalink Graduate fellowship (N.C.). We thank Karin Landrock and Dr. Brian Patrick for excellent technical assistance. N.C. also thanks Dr. Tanmaya Joshi for stimulating discussion. The HZDR is thanked for supporting the IsoSiM International Research Experience program; TRIUMF receives federal funding via a contribution agreement with the National Research Council of Canada.

■ REFERENCES

(1) Historical Timeline - SNMMI. http://www.snmmi.org/AboutSNMMI/Content.aspx?ItemNumber=4175 (accessed on January 22, 2020).

(2) Kwon, H. W.; Becker, A. K.; Goo, J. M.; Cheon, G. J. FDG Whole-Body PET/MRI in Oncology: A Systematic Review. *Nucl. Med. Mol. Imaging* **2017**, *51*, 22−31.

(3) Banerjee, S.; Ambikalmajan Pillai, M. R.; Ramamoorthy, N. Evolution of Tc-99m in Diagnostic Radiopharmaceuticals. *Semin. Nucl. Med.* **2001**, *31*, 260−277.

(4) Poty, S.; Francesconi, L. C.; McDevitt, M. R.; Morris, M. J.; Lewis, J. S. α-Emitters for Radiotherapy: From Basic Radiochemistry to Clinical Studies—Part 1. *J. Nucl. Med.* **2018**, *59*, 878−884.

(5) Poty, S.; Francesconi, L. C.; McDevitt, M. R.; Morris, M. J.; Lewis, J. S. α-Emitters for Radiotherapy: From Basic Radiochemistry to Clinical Studies—Part 2. *J. Nucl. Med.* **2018**, *59*, 1020−1027.

(6) Bartholomä, M. D. Recent Developments in the Design of Bifunctional Chelators for Metal-Based Radiopharmaceuticals Used in Positron Emission Tomography. *Inorg. Chim. Acta* **2012**, *389*, 36−51.

(7) Price, E. W.; Orvig, C. Matching Chelators to Radiometals for Radiopharmaceuticals. *Chem. Soc. Rev.* **2014**, *43*, 260−290.

(8) Brasse, D.; Nonat, A. Radiometals: towards a new success story in nuclear imaging. *Dalton Trans.* **2015**, *44*, 4845−4858.

(9) Kostelnik, T. I.; Orvig, C. Radioactive Main Group and Rare Earth Metals for Imaging and Therapy. *Chem. Rev.* **2019**, *119*, 902−956.

(10) Boros, E.; Packard, A. B. Radioactive Transition Metals for Imaging and Therapy. *Chem. Rev.* **2019**, *119*, 870−901.

(11) Holland, J. P.; Williamson, M. J.; Lewis, J. S. Unconventional Nuclides for Radiopharmaceuticals. *Mol. Imaging* **2010**, *9*, 7290.2010.00008.

(12) Tsionou, M. I.; Knapp, C. E.; Foley, C. A.; Munteanu, C. R.; Cakebread, A.; Imberti, C.; Eykyn, T. R.; Young, J. D.; Paterson, B. M.; Blower, P. J.; Ma, M. T. Comparison of macrocyclic and acyclic chelators for gallium-68 radiolabelling. *RSC Adv.* **2017**, *7*, 49586−49599.

(13) Boros, E.; Ferreira, C. L.; Cawthray, J. F.; Price, E. W.; Patrick, B. O.; Wester, D. W.; Adam, M. J.; Orvig, C. Acyclic Chelate with Ideal Properties for 68Ga PET Imaging Agent Elaboration. *J. Am. Chem. Soc.* **2010**, *132*, 15726−15733.

(14) Bergeron, R. J.; Wiegand, J.; Brittenham, G. M. HBED ligand: preclinical studies of a potential alternative to deferoxamine for treatment of chronic iron overload and acute iron poisoning. *Blood* **2002**, *99*, 3019−3026.

(15) Sathekge, M.; Lengana, T.; Modiselle, M.; Vorster, M.; Zeevaart, J. R.; Maes, A.; Ebenhan, T.; Van de Wiele, C. 68Ga-PSMA-HBED-CC PET Imaging in Breast Carcinoma Patients. *Eur. J. Nucl. Med. Mol. Imaging* **2017**, *44*, 689−694.

(16) Li, L.; de Guadalupe Jaraquemada-Peláez, M.; Aluicio-Sarduy, E.; Wang, X.; Jiang, D.; Sakheie, M.; Kuo, H.-T. E.; Barnhart, T.; Cai, W.; Radchenko, V.; Schaffer, P.; Lin, K. S.; Engle, J. W.; Bénard, F.; Orvig, C. [$^{Nat/44}$Sc(Pypa)]-: Thermodynamic Stability, Radiolabeling, and Biodistribution of a Prostate-Specific-Membrane-Antigen-Targeting Conjugate. *Inorg. Chem.* **2020**, *59*, 1985−1995.

(17) Vaughn, B. A.; Ahn, S. H.; Aluicio-Sarduy, E.; Devaraj, J.; Olson, A. P.; Engle, J.; Boros, E. Chelation with a Twist: A Bifunctional Chelator to Enable Room Temperature Radiolabeling and Targeted PET Imaging with Scandium-44. *Chem. Sci.* **2020**, *11*, 333−342.

(18) Singh, A.; van der Meulen, N. P.; Muller, C.; Klette, I.; Kulkarni, H. R.; Turler, A.; Schibli, R.; Baum, R. P. First-in-Human PET/CT Imaging of Metastatic Neuroendocrine Neoplasms with Cyclotron-Produced ^{44}Sc-DOTATOC: A Proof-of-Concept Study. *Cancer Biother.Radiopharm.* **2017**, *32*, 124−132.

(19) Huclier-Markai, S.; Alliot, C.; Kerdjoudj, R.; Mougin-Degraef, M.; Chouin, N.; Haddad, F. Promising Scandium Radionuclides for Nuclear Medicine: A Review on the Production and Chemistry up to *in Vivo* Proofs of Concept. *Cancer Biother.Radiopharm.* **2018**, *33*, 316−329.

(20) Eppard, E.; de la Fuente, A.; Benësová, M.; Khawar, A.; Bundschuh, R. A.; Gärtner, F. C.; Kreppel, B.; Kopka, K.; Essler, M.; Rösch, F. Clinical Translation and First In-Human Use of [^{44}Sc]Sc-PSMA-617 for PET Imaging of Metastasized Castrate-Resistant Prostate Cancer. *Theranostics* **2017**, *7*, 4359−4369.

(21) Opacic, T.; Paefgen, V.; Lammers, T.; Kiessling, F. Status and trends in the development of clinical diagnostic agents. *WIREs Nanomed. Nanobiotechnol.* **2017**, *9*, e1485.

(22) Lubberink, M.; Tolmachev, V.; Widström, C.; Bruskin, A.; Lundqvist, H.; Westlin, J. E. ^{110m}In-DTPA-D-Phe^{1}-Octreotide for Imaging of Neuroendocrine Tumors with PET. *J. Nucl. Med.* **2002**, *43*, 1391−1397.

(23) Kersemans, V.; Cornelissen, B.; Minden, M. D.; Brandwein, J.; Reilly, R. M. Drug-Resistant AML Cells and Primary AML Specimens Are Killed by 111In-Anti-CD33 Monoclonal Antibodies Modified with Nuclear Localizing Peptide Sequences. *J. Nucl. Med.* **2008**, *49*, 1546−1554.

(24) Aghevlian, S.; Boyle, A. J.; Reilly, R. M. Radioimmunotherapy of cancer with high linear energy transfer (LET) radiation delivered by radionuclides emitting α-particles or Auger electrons. *Adv. Drug Delivery Rev.* **2017**, *109*, 102−118.

(25) Boros, E.; Holland, J. P. Chemical Aspects of Metal Ion Chelation in the Synthesis and Application Antibody-Based Radiotracers. *J. Labelled Compd. Radiopharm.* **2018**, *61*, 652−671.

(26) Pearson, R. G. Hard and Soft Acids and Bases. *J. Am. Chem. Soc.* **1963**, *85*, 3533−3539.

(27) Shannon, R. D. Revised Effective Ionic Radii and Systematic Studies of Interatomie Distances in Halides and Chaleogenides. *Acta Crystallogr., Sect. A: Cryst. Phys., Diffr., Theor. Gen. Crystallogr.* **1976**, *A32*, 751−767.

(28) Ramogida, C. F.; Pan, J.; Ferreira, C. L.; Patrick, B. O.; Rebullar, K.; Yapp, D. T. T.; Lin, K. S.; Adam, M. J.; Orvig, C. Nitroimidazole-Containing H_2Dedpa and H_2*CHX* Dedpa Derivatives as Potential PET Imaging Agents of Hypoxia with ^{68}Ga. *Inorg. Chem.* **2015**, *54*, 4953−4965.

https://dx.doi.org/10.1021/acs.inorgchem.0c00509
Inorg. Chem. XXXX, XXX, XXX−XXX

(29) Eder, M.; Schäfer, M.; Bauder-Wüst, U.; Hull, W. E.; Wängler, C.; Mier, W.; Haberkorn, U.; Eisenhut, M. ^{68}Ga-Complex Lipophilicity and the Targeting Property of a Urea-Based PSMA Inhibitor for PET Imaging. *Bioconjugate Chem.* **2012**, *23*, 688−697.
(30) Eder, M.; Wängler, B.; Knackmuss, S.; LeGall, F.; Little, M.; Haberkorn, U.; Mier, W.; Eisenhut, M. Tetrafluorophenolate of HBED-CC: a versatile conjugation agent for ^{68}Ga-labeled small recombinant antibodies. *Eur. J. Nucl. Med. Mol. Imaging* **2008**, *35*, 1878−1886.
(31) Seemann, J.; Waldron, B. P.; Roesch, F.; Parker, D. Approaching 'Kit-Type' Labelling with 68 Ga:The DATA Chelators. *ChemMedChem* **2015**, *10*, 1019−1026.
(32) Wang, X.; de Guadalupe Jaraquemada-Pelaéz, M.; Cao, Y.; Pan, J.; Lin, K. S.; Patrick, B. O.; Orvig, C. H_2hox: Dual-Channel Oxine-Derived Acyclic Chelating Ligand for ^{68}Ga Radiopharmaceuticals. *Inorg. Chem.* **2019**, *58*, 2275−2285.
(33) Prata, M. I. M.; André, J. P.; Kovács, Z.; Takács, A. I.; Tircsó, G.; Tóth, I.; Geraldes, C. F. G. C. J. Gallium(III) chelates of mixed phosphonate-carboxylate triazamacrocyclic ligands relevant to nuclear medicine: Structural, stability and in vivo studies. *J. Inorg. Biochem.* **2017**, *177*, 8−16.
(34) Price, T. W.; Gallo, J.; Kubícek, V.; Böhmová, Z.; Prior, T. J.; Greenman, J.; Hermann, P.; Stasiuk, G. J. Amino acid based gallium-68 chelators capable of radiolabeling at neutral pH. *Dalt. Trans.* **2017**, *46*, 16973−16982.
(35) Banerjee, S. R.; Levadala, M. K.; Lazarova, N.; Wei, L.; Valliant, J. F.; Stephenson, K. A.; Babich, J. W.; Maresca, K. P.; Zubieta, J. Bifunctional Single Amino Acid Chelates for Labeling of Biomolecules with the {Tc(CO)3}+ and {Re(CO)3}+ Cores. Crystal and Molecular Structures of [ReBr(CO)3(H2NCH2C5H4N)], [Re(CO)3{(C5H4NCH2)2NH}]Br, [Re(CO)3{(C5H4NCH2)2NCH2CO2H}]Br, [Re(CO)3{X(Y)NCH2CO2CH2CH3}]Br (X = Y = 2-Pyridylmethyl; X = 2-Pyridylmethyl, Y = 2-(1-Methylimidazolyl)Methyl; X = Y = 2-(1-Methylimidazolyl)Methyl), [ReBr(CO)3{(C5H4NCH2)NH(CH2C4H3S)}], and [Re(CO)3-{(C5H4NCH2)N(CH2C4H3S)(CH2CO2)}]. *Inorg. Chem.* **2002**, *41*, 6417−6425.
(36) Nonat, A. M.; Gateau, C.; Fries, P. H.; Helm, L.; Mazzanti, M. New Bisaqua Picolinate-Based Gadolinium Complexes as MRI Contrast Agents with Substantial High-Field Relaxivities. *Eur. J. Inorg. Chem.* **2012**, *2012*, 2049−2061.
(37) Weekes, D. M.; Ramogida, C. F.; Jaraquemada-Peláez, M. D. G.; Patrick, B. O.; Apte, C.; Kostelnik, T. I.; Cawthray, J. F.; Murphy, L.; Orvig, C. Dipicolinate Complexes of Gallium(III) and Lanthanum(III). *Inorg. Chem.* **2016**, *55*, 12544−12558.
(38) Wang, X.; Jaraquemada-Peláez, M. D. G.; Rodríguez-Rodríguez, C.; Cao, Y.; Buchwalder, C.; Choudhary, N.; Jermilova, U.; Ramogida, C. F.; Saatchi, K.; Häfeli, U. O.; Patrick, B. O.; Orvig, C. H_4 octox: Versatile Bimodal Octadentate Acyclic Chelating Ligand for Medicinal Inorganic Chemistry. *J. Am. Chem. Soc.* **2018**, *140*, 15487−15500.
(39) Stasiuk, G. J.; Tamang, S.; Imbert, D.; Gateau, C.; Reiss, P.; Fries, P.; Mazzanti, M. Optimizing the Relaxivity of Gd(III) Complexes Appended to InP/ZnS Quantum Dots by Linker Tuning. *Dalton Trans.* **2013**, *42*, 8197−8200.
(40) Malyarick, M. A.; Ilyuhin, A. B.; Petrosyants, S. P. Seven- and Eight- Coordinate Complexes of Indium(III) with Nitrilotriacetate. *Main Group Met. Chem.* **1994**, *17*, 707−718.
(41) Yang, L. W.; Liu, S.; Wong, E. J.; Rettig, S.; Orvig, C. Complexes of Trivalent Metal Ions with Potentially Heptadentate N4O3 Schiff Base and Amine Phenol Ligands of Varying Rigidity. *Inorg. Chem.* **1995**, *34*, 2164−2178.
(42) Riesen, A.; Kaden, T. A.; Ritter, W.; Mäcke, H. R. Synthesis and *X*-ray structural characterisation of seven co-ordinate macrocyclic In^{3+} complexes with relevance to radiopharmaceutical applications. *J. Chem. Soc., Chem. Commun.* **1989**, *8*, 460−462.
(43) McRitchie, D. D.; Palenik, R. C.; Palenik, G. J. A pentagonal bipyramidal scandium(III) complex: Synthesis and characterization of diaqua(2,6-diacetylpyridine bis-semicarbazone)scandium(III) hydroxide dinitrate. *Inorg. Chim. Acta* **1976**, *20*, L27−L28.
(44) Carravetta, M.; Concistre, M.; Levason, W.; Reid, G.; Zhang, W. Rare Neutral Diphosphine Complexes of Scandium(III) and Yttrium(III) Halides. *Inorg. Chem.* **2016**, *55*, 12890−12896.
(45) Pniok, M.; Kubícek, V.; Havlícková, J.; Kotek, J.; Sabatie-Gogová, A.; Plutnar, J.; Huclier-Markai, S.; Hermann, P. Thermodynamic and Kinetic Study of Scandium(III) Complexes of DTPA and DOTA: A Step Toward Scandium Radiopharmaceuticals. *Chem. - Eur. J.* **2014**, *20*, 7944−7955.
(46) Nagy, G.; Szikra, D.; Trencsényi, G.; Fekete, A.; Garai, I.; Giani, A. M.; Negri, R.; Masciocchi, N.; Maiocchi, A.; Uggeri, F.; Tóth, I.; Aime, S.; Giovenzana, G. B.; Baranyai, Z. AAZTA: An Ideal Chelating Agent for the Development of 44 Sc PET Imaging Agents. *Angew. Chem., Int. Ed.* **2017**, *56*, 2118−2122.
(47) Green, M. A.; Huffman, J. C. The molecular structure of indium oxine. *J. Nucl. Med.* **1988**, *29*, 417−420.
(48) Craig, A. S.; Helps, I. M.; Parker, D.; Adams, H.; Bailey, N. A.; Williams, M. G.; Smith, J. M. A.; Ferguson, G. Crystal and Molecular Structure of a Seven- Coordinate Chloroindium(III) Complex of 1,4,7-Triazacyclononanetriacetic Acid. *Polyhedron* **1989**, *8*, 2481−2484.
(49) Gans, P.; Sabatini, A.; Vacca, A. Determination of equilibrium constants from spectrophometric data obtained from solutions of known pH: The program pHab. *Ann. Chim.* **1999**, *89*, 45−49.
(50) Li, L.; de Guadalupe Jaraquemada-Pelaéz, M.; Kuo, H. T.; Merkens, H.; Choudhary, N.; Gitschtaler, K.; Jermilova, U.; Colpo, N.; Uribe-Munoz, C.; Radchenko, V.; Schaffer, P.; Lin, K. S.; Benard, F.; Orvig, C. Functionally Versatile and Highly Stable Chelator for ^{111}In and ^{177}Lu: Proof-of-Principle Prostate-Specific Membrane Antigen Targeting. *Bioconjugate Chem.* **2019**, *30*, 1539−1553.
(51) Cram, D. J. Preorganization- From Solvents to Spherands. *Angew. Chem., Int. Ed. Engl.* **1986**, *25*, 1039−1057.
(52) Harris, W. R.; Carrano, C. J.; Raymond, K. N. Spectrophotometric Determination of the Proton-Dependent Stability Constant of Ferric Enterobactin. *J. Am. Chem. Soc.* **1979**, *101*, 2213−2214.
(53) Price, E. W.; Cawthray, J. F.; Bailey, G. A.; Ferreira, C. L.; Boros, E.; Adam, M. J.; Orvig, C. H4octapa: An Acyclic Chelator for 111In Radiopharmaceuticals. *J. Am. Chem. Soc.* **2012**, *134*, 8670−8683.
(54) Clevette, D. J.; Orvig, C. Comparison of Ligands of Differing Denticity and Basicity for the *in Vivo* Chelation of Aluminium and Gallium. *Polyhedron* **1990**, *9*, 151−161.
(55) Bardez, E.; Devol, I.; Larrey, B.; Valeur, B. Excited-State Processes in 8-Hydroxyquinoline: Photoinduced Tautomerization and Solvation Effects. *J. Phys. Chem. B* **1997**, *101*, 7786−7793.
(56) Xu, H.; Baidoo, K.; Gunn, A. J.; Boswell, C. A.; Milenic, D. E.; Choyke, P. L.; Brechbiel, M. W. Design, synthesis, and characterization of a dual modality positron emission tomography and fluorescence imaging agent for monoclonal antibody tumor-targeted imaging. *J. Med. Chem.* **2007**, *50*, 4759−4765.
(57) Ramogida, C. F.; Murphy, L.; Cawthray, J. F.; Ross, J. D.; Adam, M. J.; Orvig, C. Novel "bi-modal" H_2 dedpa derivatives for radio- and fluorescence imaging. *J. Inorg. Biochem.* **2016**, *162*, 253−262.
(58) Bhushan, K. R.; Misra, P.; Liu, F.; Mathur, S. E.; Lenkinski, R. V.; Frangioni, J. Detection of Breast Cancer Microcalcifications Using a Dual-modality SPECT/ NIR Fluorescent Probe. *J. Am. Chem. Soc.* **2008**, *130*, 17648−17649.
(59) Thorp-Greenwood, F. L.; Coogan, M. P. Multimodal radio-(PET/SPECT) and fluorescence imaging agents based on metallo-radioisotopes: current applications and prospects for development of new agents. *Dalton Trans.* **2011**, *40*, 6129−6143.
(60) Ahn, S. H.; Boros, E. Nuclear and Optical Bimodal Imaging Probes Using Sequential Assembly: A Perspective. *Cancer Biother.Radiopharm.* **2018**, *33*, 308−315.
(61) Wang, F.; Banerjee, D.; Liu, Y.; Chen, X.; Liu, X. Upconversion nanoparticles in biological labeling, imaging, and therapy. *Analyst* **2010**, *135*, 1839−1854.

https://dx.doi.org/10.1021/acs.inorgchem.0c00509
Inorg. Chem. XXXX, XXX, XXX−XXX

(62) Koole, R.; Mulder, W. J.; van Schooneveld, M. M.; Strijkers, G. J.; Meijerink, A.; Nicolay, K. Magnetic quantum dots for multimodal imaging. *Wiley Interdiscip. Rev. Nanomed. Nanobiotechnol.* **2009**, *1*, 475−491.
(63) Arrowsmith, R. L.; Waghorn, P. A.; Jones, M. W.; Bauman, A.; Brayshaw, S. K.; Hu, Z.; Kociok-Köhn, G.; Mindt, T. L.; Tyrrell, R. M.; Botchway, S. W.; Dilworth, J. R.; Pascu, S. I. Fluorescent gallium and indium bis(thiosemicarbazonates) and their radiolabelled analogues: Synthesis, structures and cellular confocal fluorescence imaging investigations. *Dalton Trans.* **2011**, *40*, 6238−6252.
(64) Rieffel, J.; Chitgupi, U.; Lovell, J. F. Recent Advances in Higher-Order, Multimodal, Biomedical Imaging Agents. *Small* **2015**, *11*, 4445−4461.
(65) Satpati, D.; Sharma, R.; Sarma, H. D.; Dash, A. Comparative Evaluation of ^{68} Ga-Labeled NODAGA, DOTAGA, and HBED-CC-Conjugated CNGR Peptide Chelates as Tumor-Targeted Molecular Imaging Probes. *Chem. Biol. Drug Des.* **2018**, *91*, 781.
(66) Kularatne, S. A.; Zhou, Z.; Yang, J.; Post, C. B.; Low, P. S. Design, Synthesis, and Preclinical Evaluation of Prostate-Specific Membrane Antigen Targeted 99mTc-Radioimaging Agents. *Mol. Pharmaceutics* **2009**, *6*, 790−800.
(67) Zhang, Z.; Rettig, S. J.; Orvig, C. Contribution from the Lipophilic Coordination Compounds: Aluminum, Gallium, and Indium Complexes of l-Aryl-3-hydroxy-2-methyl-4-pyridinones. *Inorg. Chem.* **1991**, *30*, 509−515.
(68) Harris, W. R.; Pecoraro, V. L. Thermodynamic binding constants for gallium transferrin. *Biochemistry* **1983**, *22*, 292−299.
(69) Zarschler, K.; Kubeil, M.; Stephan, H. Establishment of two complementary *in vitro* assays for radiocopper complexes achieving reliable and comparable evaluation of *in vivo* stability. *RSC Adv.* **2014**, *4*, 10157−10164.
(70) Harris, W. R.; Chen, Y.; Wein, K. Equilibrium Constants for the Binding of Indium(III) to Human Serum Transferrin. *Inorg. Chem.* **1994**, *33*, 4991−4998.
(71) Choudhary, N.; Dimmling, A.; Wang, X.; Southcott, L.; Radchenko, V. O.; Patrick, B.; Comba, P.; Orvig, C. Octadentate Oxine-Armed Bispidine Ligand for Radiopharmaceutical Chemistry. *Inorg. Chem.* **2019**, *58*, 8685−8693.
(72) Gran, G. Determination of the equivalence point in potentiometric titrations. Part II. *Analyst* **1952**, *77*, 661−671.
(73) Baes, C. F., Jr.; Mesmer, R. S. *The Hydrolysis of Cations*; John Wiley & Sons: New York, 1976.
(74) Sheldrick, G. M. Crystal structure refinement with SHELXL. *Acta Crystallogr., Sect. C: Struct. Chem.* **2015**, *71*, 3−8.
(75) Dolomanov, O. V.; Bourhis, L. J.; Gildea, R. J.; Howard, J. A. K.; Puschmann, H. OLEX2: a complete structure solution, refinement and analysis program. *J. Appl. Crystallogr.* **2009**, *42*, 339−341.
(76) Burla, M. C.; Caliandro, R.; Camalli, M.; Carrozzini, B.; Cascarano, G. L.; Giacovazzo, C.; Mallamo, M.; Mazzone, A.; Polidori, G.; Spagna, R. SIR2011: a new package for crystal structure determination and refinement. *J. Appl. Crystallogr.* **2012**, *45*, 357−361.

https://dx.doi.org/10.1021/acs.inorgchem.0c00509
Inorg. Chem. XXXX, XXX, XXX−XXX